# Flow cytometry has a significant impact on the cellular metabolome

Aleksandra Binek[1]‡, David Rojo[2]‡, Joanna Godzien[2], Francisco Javier Rupérez[2], Vanessa Nuñez[1], Inmaculada Jorge[1,3], Mercedes Ricote[1], Jesús Vázquez[1,3], Coral Barbas[2]*

[1] Fundación Centro Nacional de Investigaciones Cardiovasculares Carlos III, Madrid, Spain[1]

[2] Centro de Metabolómica y Bioanálisis (CEMBIO), Facultad de Farmacia, Universidad CEU San Pablo, Campus Montepríncipe, Madrid, Spain

[3] CIBER de Enfermedades Cardiovasculares (CIBER CV), Madrid, Spain

‡These authors contributed equally to this work

* Correspondence and requests for materials should be addressed to:

Coral Barbas (cbarbas@ceu.es)

Centro de Metabolómica y Bioanálisis (CEMBIO), Facultad de Farmacia

Universidad CEU San Pablo, Campus Montepríncipe

Boadilla del Monte

28668 Madrid, Spain

**ABSTRACT**

The characterization of specialized cell subpopulations in a heterogeneous tissue is essential for understanding organ function in health and disease. A popular method of cell isolation is fluorescence-activated cell sorting (FACS) based on probes that bind surface or intracellular markers. In this study, we analyse the impact of FACS on the cell metabolome of mouse peritoneal macrophages. Compared with directly pelleted macrophages, FACS-treated cells had an altered content of metabolites related to the plasma membrane, activating a mechanosensory signalling cascade causing inflammation-like stress. The procedure also triggered alterations related to energy consumption and cell damage. The observed changes mostly derive from the physical impact on cells during their passage through the instrument. These findings provide evidence of FACS-induced biochemical changes, which should be taken into account in the design of robust metabolic assays of cells separated by flow cytometry.

**KEYWORDS**

Sorting, sorted cells, metabolome profile, fluorescence activated cell sorting (FACS), LC-MS, CE-MS, GC-MS, metabolomics, multiplatform analysis

## INTRODUCTION

The functional properties of any tissue are always the product of the contributions of its specialized cells. Analysing the molecular profiles of these cell types usually requires the isolation of functionally homogeneous cell subpopulations using methods compatible with subsequent analytical approaches. Fluorescence-activated cell sorting (FACS) is one of the most routinely used and well-established procedures for isolating and counting cell populations before further procedures such as cell culture[1-3], metabolic assay[1, 2], mRNA expression analysis[1, 4, 5], phenotypic characterization[2, 4], and other high-throughput approaches[6, 7]. Since its introduction in the 70s[8], the research applications of FACS have been broad, and have recently included metabolic characterization[2, 4, 9-12]. The core cell phenotype assays include the assessment of glycolytic activity from glucose concentrations, together with functional evaluations (cell motility, accumulation or distribution), and mRNA/protein expression quantifications. Enhanced glycolysis has been shown to influence endothelial-cell glucose availability in FACS-sorted hypoxic tumour-associated macrophages harvested from tumour-bearing mice[2]. In another example of metabolic characterization, the levels of ribose-5-phosphate, ribulose-5-phosphate, and glutathione (with detection of significant changes in all 3 metabolites) were measured in sorted CD8+ T cells by high throughput metabolomic profiling[4]. Despite the ability of FACS to isolate specific cell populations, it remains unclear to what extent the sorting process itself induces changes in cell function.

The cell metabolome responds rapidly and dynamically to external alterations, and metabolomics is thus the most suitable approach to assessing the effect of FACS-triggered

stimuli. Using cellular cultures, two studies have partially evaluated the impact of FACS on cell metabolism[13, 14]. Roci *et al*. (2016)[13] have focused on the traceability of certain polar isotopically labelled-metabolites, comparing extracted cell from a dish, pelleted cells and sorted cells. Meanwhile, oxidative stress has been the centre of the research by Llufrio *et al.* (2018)[15] , comparing quick quench, delayed-quench and sorted cells. Here, we present a systematic evaluation of the impact of FACS analysis on cell metabolism, using peritoneal macrophages from mice as a cell model, which better mimics the circumstances applicable in an *in vivo* experiment. We used a multiplatform mass spectrometry (MS) approach, maximizing metabolite coverage by combining liquid chromatography (LC), capillary electrophoresis (CE), and gas chromatography (GC) as separation techniques. We show that, compared with direct pelleting of peritoneal lavage, FACS sorting of peritoneal macrophages alters around 10% of metabolic features, most of them associated with the flow cytometry process and not the immunostaining. Changes observed in our data could be attributed to the physical stress of cell sorting, which in turn might induce a mechanosensory signalling cascade that alters the abundance of glycerophospholipids, fatty acyls, fatty acid esters, amino acids (and derivatives), glycerolipids, and sphingolipids. The overall effect can be interpreted as a mechanically induced inflammatory-like status involving calcium ($Ca^{2+}$) signalling[16-19] and mechanosensitive phospholipase A2 (PLA2) translocation to the cell membrane[20, 21] together with energy consumption and cell damage, potentially compromising cell homeostasis. These and previous studies[2, 14, 22] results demonstrate that the cell sorting

process itself induces marked changes in the cell machinery that may interfere with the molecular processes being analysed.

## METHODS

***Study design***. Four experimental group of thioglycollate-induced peritoneal macrohpages were prepared, with 5 biological replicates each (n=20) (Figure 1). In total, 20 animals (10 females and 10 males) were sacrificed to produce sufficient peritoneal macrophages for metabolome fingerprinting (Supplementary Table S1). Sample size was chosen based on the number of cells necessary to perform high quality metabolite extraction and multiplatform MS analysis. Samples were normalized by adding an extraction volume proportional to the mass of the cell pellet. The cell number necessary to perform the metabolomics experiments was estimated to produce a dry cellular pellet weight within the range 30-100mg, an amount that represents the protocols applied by different groups[23-26]. The exact cell number used for the metabolite extraction is specified in Supplementary Table S1. No animal randomization was performed in assigning experimental groups. The control experimental group (Ctrl) was composed of peritoneal lavage pelleted cells immediately snap-frozen in liquid nitrogen (liq. $N_2$) upon isolation. The antibody sample group (Ab) consisted of peritoneal macrophages subjected to immunostaining and subsequently stored in liq. $N_2$ without sorting. The sorted sample (Sort) consisted of freshly isolated macrophages immediately analysed by flow cytometry without antibody labelling and with sorting of the complete cell population into the collection tube. For the antibody-stained and sorted sample (Ab+Sort), the freshly isolated cells were immunostained and then sorted by flow cytometry, with collection of the complete cell population. No subpopulations were isolated in order to ensure that sample composition remained comparable to the Ctrl and Ab groups and to identify biochemical

changes induced solely by the sorting process. After collection, cells from the Sort and Ab+Sort group were pelleted, frozen in liq. $N_2$, and stored at -80°C until fingerprinting analysis.

***Animals***. C57BL/6 mice were provided by Charles River. Mice were housed under identical environmental conditions, including feeding, light, and temperature. All animal procedures were approved by the Experimental Animal Use Committee of the Instituto de Salud Carlos III and were in accordance with the EU Directive 86/609.

***Peritoneal macrophages isolation and flow cytometry***. The isolation protocol and flow cytometry are detailed in Supplementary Methods.

***Reagents and standards for metabolomics***. Reagents and standards are detailed in Supplementary Methods.

***Metabolite extraction and sample treatment***. Since biological replicates differed slightly in cell number, the extraction solvent volume was calculated according to the cell pellet mass, thus ensuring between-sample normalization of metabolite concentrations (Supplementary Table S1). On the day of analysis, cell pellets were thawed and doubly extracted by sequential additions of i) MeOH:MTBE (4:1, v/v) and ii) MeOH:$H_2O$ (4:1, v/v). Each solvent addition was followed by 3 cycles of freeze/thawing (liq. $N_2$ /cold-water bath, 10 s), sonication (15 W, 6 min), vortexing (1 min), and centrifugation (16,000 g, 10 min, 4°C). Equal volumes of the supernatants from i and ii were then mixed and aliquoted for subsequent analysis. Details about the sample treatment per analytical platform can be found in Supplementary Methods.

***Preparation of quality controls (QCs)***. QC samples are required at the beginning of the sequence to stabilize the system and throughout the analytical runs at periodic intervals to monitor variations in signals over time. Individual QC samples were therefore prepared independently for each analytical platform by pooling and mixing equal volumes of each - sample. After gentle vortexing, the mixes were transferred to analytical vials. Detailed information about the injection order and the number of blanks and QCs used to stabilize each analytical platform can be found in Supplementary Methods.

***Metabolomic fingerprinting***. To maximize metabolite coverage, samples were run on 3 analytical platforms: general and lipidomic (adapted from Whiley *et al.* (2012)[27]) LC-ESI-QTOF-MS methods, CE-ESI-TOF-MS, and GC-EI-Q-MS (using the FiehnLib[28] and NIST 14 libraries). Detailed methodology can be found in Supplementary Methods.

***Metabolomic data treatment, statistical analysis, and identification***. In LC-MS and CE-MS, data were deconvoluted with the Molecular Feature Extraction algorithm in the MassHunter Qualitative Analysis software (B.06.00, Agilent). Raw data were aligned with Mass Profiler Professional (version 13.0, Agilent). In GC-MS, deconvolution and identification were performed using MassHunter Quantitative Unknowns Analysis (B.07.00, Agilent), data were aligned with MassProfiler Professional (version 13.0, Agilent) and peaks were integrated using MassHunter Quantitative Analysis software (version B.07.00, Agilent). Metabolite identification was based on the FiehnLib[28] and NIST 14 libraries.

In order to perform the differential analysis on the metabolomics data, in all the platforms the raw variables were then filtered according to a modification of the filtering criteria

proposed by Godzien *et al.* (2014)[29]: variables present in at least 50% of the samples of each experimental group and either i) present in at least 80% of the QCs that yielded a variation coefficient <30% or ii) present in <20% of the QCs. Principal component analysis (PCA) models (Supplementary Figure S1) were subsequently built using the SIMCA-P+ software (12.0.1.0, Umetrics, Sweden). For each PCA, $R^2$ (fraction of the explained variance of the model) is reported in Supplementary Figure S1. Next, after replacement of missing values by k-means nearest neighbour analysis according to the criteria of Armitage *et al.* (2015)[30], the Mann-Whitney U test was used for all comparisons (i.e., Ctrl vs Ab; Ctrl vs Sort; and Ctrl vs Ab+Sort) followed by the Benjamini-Hochberg post hoc correction ($p < 0.05$). Missing values were imputed and statistical comparisons made using in-house built scripts for MATLAB (7.10.0.499, MathWorks, Natick, MA, USA). In LC-MS and CE-MS, the resulting list of accurate masses that significantly differed between groups was searched using the CEU Mass Mediator search tool (http://biolab.uspceu.com/mediator; error ± 5 ppm) to obtain tentative identifications, taking into account mass accuracy, possibility of ion formation and adducts formations. Each identification was then manually curated based on MS adducts[31] for lipids identified by LC-MS (MS/MS validated criteria[32]) and on the in-source fragmentation pattern[33] for metabolites identified by CE-MS. When appropriate, the elution order was considered in order to discard spurious identifications. The number of hits per analytical platform that passed each step is listed in Supplementary Table S2. The biological role of identified compounds was evaluated and irrelevant identifications such as pesticides, drugs, or impossible chemical structures were excluded. In the final list (Supplementary Table S3), metabolites are reported according to

the criteria of the Metabolomics Standards Initiative[15, 34], with a confidence level in grade 1 (identified metabolites) (GC-MS) or grade 2 (putatively annotated compounds) (LC-MS and CE-MS). Variation between experimental conditions is reported as $\log_2$ FC, always relative to control, and will be referred to as FC in the rest of the text.

To assess the complete metabolite profile, in all the platforms the raw variables were then filtered based on a 100 % presence per group and the subsequent list searched using the CEU Mass Mediator search tool (http://biolab.uspceu.com/mediator; error ± 5 ppm) for LC-MS and CE-MS data. This dataset was considered the full detected metabolic profile. The number of annotated hits per analytical platform is listed in Supplementary Table 2.

***Hierarchical clustering analysis (HCA)*** The MetaboAnalyst online platform (http://www.metaboanalyst.ca/)[35] was used for HCA analysis of the metabolites represented in Figure 3 and Supplementary Figures S4 and S5. No normalization algorithm was applied to the data. The datasets were scaled using the auto scaling feature in the program (mean-centred and divided by the standard deviation of each variable) and graphically represented as heatmaps.

***Metabolic pathways over-representation analysis*** The MetaboAnalyst Pathway Analysis node (http://www.metaboanalyst.ca/)[35] was used to perform the analysis. The selected analysis method of over-representation was hypergeometric test.

***Data availability.*** Mass spectrometry data from this study were deposited to the publically available MetaboLights repository (https://www.ebi.ac.uk/metabolights) with the data set identifiers MTBLS633, MTBLS634, MTBLS631 and MTBLS629.

## RESULTS AND DISCUSSION

### *Overall impact of flow cytometry on the metabolome*

A multiplatform fingerprinting experiment was conducted to assess if the immunostaining and flow cytometry induced metabolic alterations in mouse peritoneal macrophages. To assess the effect of each possible source of alterations individually, we designed an experiment to evaluate the effect of immunostaining (Ab), flow cytometry (Sort), and the both elements in combination (Ab+Sort) with respect to control (Ctrl) (Figure 1). Principal components analysis (PCA) established a major distinction between 2 sample blocks respectively integrated by i) Ab and Ctrl and ii) Sort and Ab+Sort (Supplementary Figure S1).

Studying the sample clustering following a deduction approach[36], the grouping of the Ab experimental group with Ctrl in sample block i suggests that immunostaining has only a minor impact on the metabolome. Only PCA of capillary electrophoresis-mass spectrometry (CE-MS) data (Supplementary Figure S1c) revealed a slight distinction between them. Conversely, the clustering in sample block ii indicates that similar metabolic alterations take place in the Sort and Ab+Sort experimental groups, suggesting an effect of the flow cytometer instrumentation. A total of 4418 annotable metabolic features were detected, present in all samples in each group; of the total, 409 features showed alterations (9%). Relative to Ctrl samples, Ab samples showed induced changes in only 8 features, whereas Sort altered 290 features and Ab+Sort 268. Details on the number of the metabolic features passing each filtering criteria are shown in Supplementary Table S2. The PCA analysis revealed that the main origin of the metabolic

disturbances was the flow cytometry procedure and not the immunostaining (Supplementary Figure S1g). The numbers of altered metabolites with an annotated identification in each analytical platform were as follows: LC-MS (positive and negative polarity, general and lipidomic gradient), 340 (225 Ctrl vs Sort, 225 Ctrl vs Ab+Sort); CE-MS, 57 (8 Ctrl vs Ab, 57 Ctrl vs Sort, 31 Ctrl vs Ab+Sort); and GC-MS, 12 (8 Ctrl vs Sort, 12 Ctrl vs Ab+Sort). Note that the differences in the number of metabolites detected are related to the technical specification and data treatment workflow of each analytical platform.

Flow cytometry caused changes in around 10% of the identifiable metabolites, most of them produced by exposure of cells to the intrinsic mechanical stimuli related to the hydraulic system of the instrument, including stretch, pressure, and osmotic changes.

***Multiplatform analysis validation***

The robustness of the multiplatform analytical approach was demonstrated by the tight clustering of the quality controls (QCs) in the nonsupervised PCA models (plotted in Supplementary Figure S1). This confirms that among-group separation was due to real biological variability and not analytical variance. Moreover, samples are almost evenly clustered across analytical platforms.

Of the 409 altered metabolite features (Supplementary Table S2), 31 were found in 2 or 3 analytical platforms (Supplementary Figure S2). The LC-MS platforms detected 26 altered metabolites in common, the CE and LC platforms detected 5, and the GC and LC platforms detected just 1. Only 2 compounds were co-detected by all 3 analytical platforms. The detection of 345 altered metabolites (84%) with a single analytical

technique shows the importance of maximizing metabolite coverage with a multiplatform approach. All co-detected metabolites (per comparison) confirm the trend of change ($log_2$ fold change (FC)) between analytical platforms, validating the multiplatform results (Figure 2, complete set of box plots in Supplementary Figure S3). As demonstrated in Figure 2, the metabolites were selected to illustrate several changes in various metabolite classes with distinct physical and chemical properties. These results provide inter-platform validation of downregulated high energy metabolism compounds (creatine, linoleyl carnitine), nucleic acid metabolism (hypoxanthine, IMP) as well as an example of cellular membrane structural components (lysophospholipids).

***Biochemical nature of flow cytometry-induced metabolite alterations***

Most of the alterations (71% of significantly changed metabolites) were directly related to the sorting procedure (Supplementary Figure S1g), whereas 29% resulting from the combined effect of immunostaining and FACS. Peptides (subgroup of the Human Metabolome Database (HMDB) Sub Class amino acids, peptides, and analogues) were excluded from this dataset and from further biochemical interpretations because peptide abundances may be randomly affected by the partial deproteinization during metabolite extraction (Figure 3b), which should be considered a potential limitation. The 10 most abundant altered HMDB metabolite subclasses in the Sort vs Ctrl comparison were glycerophospholipids, amino acids and derivatives, fatty acid esters, sphingolipids, glycerolipids, carboxylic acids and derivatives, fatty acyls, fatty acids and conjugates, purine ribonucleotides, and eicosanoids (Figure 3c). Similarly, the combination of Ab+Sort vs Ctrl influenced the same biochemical classes in slightly different proportions (Figure 3c).

***Mechanosensitivity translates into cell stress***

The most prominent changes detected in the Sort and Ab+Sort conditions involve bioactive lipid mediators, phospholipases, membrane excision by-products, and their potential precursors. Arachidonic acid (AA), a 20-carbon omega-6 polyunsaturated fatty acid (20:4, n-6) is esterified to glycerol in cell membranes, and its enzymatic hydrolysis mediates the release of signalling and regulatory molecules. The Sort and Ab+Sort groups showed alterations in AA-derived eicosanoids, including cyclooxygenase (COX)-derived prostaglandins (PGs) and lipoxygenase (LOX)-derived leukotrienes (LTs), as well as fatty acyl and lineolic acid derivatives. FACS increased PG and LT precursors as well as other AA oxygenation pathway products (eicosanoids of exact masses: 312.1739 Da, 322.2503 Da, 336.2297 Da, 338.2453 Da, 396.2876 Da, 405.2864 Da and 571.474 Da with the same trend), suggesting consumption of the AA intermediate pool for further modifications in lipid mediator pathways (Figure 4 and Supplementary Table S3). Moreover, the Sort group showed abundance changes in linoleic acid (LA) (18:2, n-6), another major lipid mediator precursor (Figure 4). LA is processed into bioactive molecules by various COXs and LOXs through a series of oxidations and stereoisomeric conversions[37].

The phospholipid hydrolysis induced by mechanical PLA2 activation liberates not only AA, but also a variety of polyunsaturated fatty acids (PUFAs) such as eicosapentaenoic acid (EPA) and docosahexaenoic acid (DHA), leaving lysophospholipids (LysoPC) as a by-product[38]. DHA was found increased by sorting (Figure 4 and Supplementary Table S3). The detected increased abundance of LysoPC (20:4) (Figure 4 and Supplementary Table S3) in the Ab-Sort group can also be considered a major source

283 of AA, which then can be enzymatically scavenged further through the activity of
284 lysophospholipase (LPL) as one possible AA metabolic pathway.
285 Our results also show an effect of sorting on the activity of other phospholipases.
286 While PLA2 releases AA in a single-step reaction, phospholipase C (PLC) and D (PLD)
287 produce the AA-containing lipid products diacyglycerols (DG) and phosphatidic acids (PA),
288 respectively. Sorting decreased the abundance of the DG family members DG(44:12)
289 (depleted in Ab+Sort), DG(36:5) (FC -1.52), DG(36:2) (FC -1.64), DG(38:5) (FC -1.59),
290 DG(40:4) (FC -1.40), DG(42:8) (FC -1.60), DG(36:8) (FC -0.95), DG(P-32:1) (depleted in
291 Ab+Sort), DG(34:2) (FC -1.58), DG(36:4) (depleted in Ab+Sort), DG(38:7) (FC -1.39),
292 DG(38:4) (FC -1.54), DG(40:7) (FC -1.48), DG(42:10) (FC -1.32), DG(40:3) (FC -1.18), and
293 increased species DG(32:3) (appeared in Ab+Sort, when absent in Ctrl), DG(34:5) (FC 1.09
294 in Sort), altogether possibly reflecting PLC and DG lipase activity. PLC activity was
295 previously found to depend upon periodic mechanical stress, electrostatic potential, and
296 elastic stress of lipid membranes[39-41]. The observed increase in DG consumption in FACS
297 sorted macrophages might be associated with PLC and DG lipase activities, which are
298 crucial in the biosynthesis of 2-arachidonoylglycerol (2-AG)[42, 43], the AA precursor in the
299 endocannabinoid signalling pathway[43]. The outcome is an inflammatory-like status
300 featuring increased energy consumption and cell damage, potentially compromising cell
301 homeostasis. The Sort and Ab+Sort groups also showed decreases in several PUFAs,
302 including anandamide (20:4, n=6) (AEA) (FC -3.87), anandamide (20:5, n=3) (EPEA) (FC -
303 3.88), and increase in anandamide (20:1, n=9) (FC 0.97). Moreover, Ab+Sort showed an

increase in the antiinflammatory mediator resolvin. These findings might suggest an effort of cells to cope with inflammation-like conditions induced by the sorting process.

Another key finding is the marked change in the phospholipid profile of the cell membrane. The decreased glycerophospholipid content in the Sort and Ab+Sort groups could be explained by mechanical rupture of the plasma lipid bilayer and the activation of phospholipases possibly hydrolysing the membrane phospholipid pool to release stress-activated bioactive lipid mediators. For example, the decreased abundance in Sort and Ab+Sort samples of highly unsaturated PC and PI species (≥4 double bonds: PC(36:5) (depleted in Ab+Sort), PC(38:4) (FC -0.43), PC(38:7) (FC -3.20), PC(40:6) (FC -0.67), PC(40:7) (FC -3.36), PC(42:6) (depleted in Ab+Sort), PC(44:6) (FC -1.03), PI(38:5) (FC -0.65), PI(40:4) (FC -7.82), PI(42:4) (FC -1.06), and PI(36:5) (FC -1.02)) could be related to PLA2-mediated intracellular cleavage of AA. In resting human monocytes, PC and PE typically constitute the major reservoirs of AA (43% and 39% of total phospholipid AA, respectively), with a lower AA content in PI (18%)[44]. In a recent study, Balgoma *et al.* (2010) reported that monocyte activation decreased the content of AA-containing PC and PI species while having no effect on PE species[44]. In another study, Shamsuddin *et al.* (2015) found that PI are the primary source of AA-derived signalling eicosanoids[45]. The observed changes in PC and PI species in our study point into a direction of a possible consumption of highly unsaturated phospholipids mediated by phospholipase activity. However, sorted mouse peritoneal macrophages also showed decreased abundance of several PE species (PE(36:5) (FC -0.64), PE(38:4) (FC -0.99), PE(38:5) (FC -0.80), PE(38:6) (FC -0.84), PE(38:7) (FC -0.93), PE(40:4) (FC -1.15), PE(40:5) (FC -1.10), PE(40:6) (FC -0.84), PE(40:7) (depleted in Sort), and

PE(40:9) (depleted in Sort)). These results were also confirmed in the biological pathways over-representation analysis that showed phosphatidylcholine and phosphatidylethanolamine biosynthesis pathways being substantially impacted by sorting (Supplementary Figure S4). Several lyso-PE and lyso-PC forms were also altered, with a general tendency to decrease (Figure 4 and Supplementary Table S3). Lysophospholipids are produced by the enzymatic action of membrane phospholipases. Interestingly, Lyso-PE(24:6) was the only PE species increased in the Sort and Ab+Sort groups and was completely absent in Ctrl macrophages (Figure 4), it might be considered as a potential new intermediate source of PUFAs. In addition to PE, PI, and PC species and lysolipids, sorting also induced a marked downregulation in several phosphatidylserine (PS) species (Figure 4 and Supplementary Table S3). PS are glycerophospholipids, accounting for 10%-20% of the total phospholipid content of the plasma membrane and playing crucial roles in nonspecific electrostatic interactions[46] and apoptosis[47].

The flow cytometry procedure also triggered depletion of several gangliosides and sphingomyelins (SM) (Figure 4 and Supplementary Table S3). Gangliosides are glycosphingolipids with a sugar side chain that modulates cell signal transduction events in the cell plasma membrane[48]. The abundance decrease in several SM species (SM(d40:2), SM(d40:3), SM(d42:1) and SM(d44:2)) may be related to sphingomyelinase (SMase) mechanoactivation, which is known to initiate the generation of ceramides (Cer)[49, 50]. Consistent with this idea, the decreased abundance of SM(d40:2), SM(d42:1)) in the Sort group coincided with increased abundance of in the corresponding ceramides Cer(d40:2) Cer(d42:1) (Figure 4 and Supplementary Table S3). Ceramides play roles in the

biosynthesis of glycosphingolipids and gangliosides, lipid bilayer components and are important inducers of apoptosis[51, 52]. Another FACS-upregulated lipid species was phytosphingosine (FC 2.34), which is involved in diverse cell processes, including cell-cell interaction, proliferation, differentiation, and apoptosis[53].

***Depleted cell energy generation and storage***

Energy metabolism is directly linked to the maintenance of cell homeostasis. Our analysis indicated that FACS induces consumption of ATP and ADP (in agreement with Llufrio et al. (2018)[14]), correlating with AMP accumulation (FC 0.55) and depletion of adenosine, creatinine (FC -1.62), and creatine (FC -2.2), the main compounds involved in ATP recycling (Supplementary Table S3). These alterations were also reflected in the metabolic pathways over-representation analysis that indicated FACS impact on purine metabolism (Supplementary Figure S4). An increased energy demand in Sort and Ab+Sort groups is also suggested by an imbalance in the tricarboxylic-acid cycle, with decreased levels of citrate/isocitrate (FC 1.44), aconitate (depleted), malate (FC -1.62), fumarate (FC -5.31), and related compounds as succinic semialdehyde (FC -1.91) and succinic anhydride (depleted). Moreover, FACS also decreased peritoneal macrophage levels of glucose (FC -1.47) and maltose (FC -2.18), consistent with consumption of the polysaccharide precursors UDP-glucose, UDP-galactose, and UDP-galactofuranose (FC -1.43). The parallel depletion of niacinamide (FC -2.19) (also in Llufrio *et al.* (2018)[14]) could indicate its potential use to synthesize NAD. Sorted cells also showed a clear alteration in lipid β-oxidation, manifested as a depletion in 12 and significant decrease in additional 11

carnitine-conjugated species (FCs in Supplementary Table S3 and in metabolic pathways over-representation analysis, Supplementary Figure S4).

***Signatures of cell damage***

Sorting increased the cell content of ADP-ribose, which is involved in the detection and signalling of single-strand DNA breaks typically caused by metabolic or chemical damage or radiation exposure[54]. This was matched by accumulation of the ribose derivatives, ribose 1-P and ribose 5-P which are structural components of DNA and RNA. Possible damage to the genetic material was also supported by the observed decrease of acetyl adenylate levels (FC -1.91), a metabolite involved in non-enzymatic histone acetylation[55]. In addition, sorting probably induced an increase in cellular oxidative stress. Glutathione, the main cellular antioxidant agent, was found decreased (FC -2.4), as were ornithine (FC -1.06), proline (FC -1.2), citrulline (FC -1.39), acetylspermidine (FC -2.08) and S-glutathionycysteine (FC -1.88), all of which are necessary for glutathione synthesis via the polyamine pathway. Consistent with these findings, sorting also decreased histidine (FC -1.36), whose imidazole ring has the capacity to scavenge reactive oxygen species (ROS)[22, 56]. Moreover, many PC and PE species were detected in their oxidized forms (sn-1 position ether bond) in sorted macrophages (PE-O and PC-O species FCs in Supplementary Table S3). Increased PC and PE oxidation could indicate upregulated synthesis of carboxy-ethyl-hydroxy-chroman (alpha and gamma-CEHC) (FC 0.80 and FC 3.38) antioxidants (for complete list of all PC and PE species see Supplementary Table S3). The overall imbalance in nucleic-acid related metabolites and the potential oxidase/antioxidant imbalance suggest cell damage due to increased ROS production upon exposure of cells to laser

391 radiation during FACS. These findings are in agreement with Llufrio *et al.* (2018)[14] , who
392 have detected that FACS significantly increases the ratio of oxidized/reduce glutathione as
393 well as ROS.

394 ***Sorting vs Ab-Sorting***

395 In general, the Ab+Sort procedure had substantial impact on macrophage
396 metabolism beyond that induced by sorting alone (see Figure 3a and 3c). Of the 251
397 annotated metabolites significantly altered by Ab+Sort, 142 are also affected in the Sort
398 group (Supplementary Figure S1g). A closer inspection clearly revealed a shared pattern of
399 change within this group of annotated metabolites in the Ab+Sort and Sort groups,
400 identifying 2 highly characteristic clusters (Figure 3a and Supplementary Figure S5). In
401 both comparisons, metabolites showing a decrease in the Ab+Sort and Sort groups are
402 generally related to energy metabolism, including energy source catabolism, storage, and
403 transfer. This subset includes carnitine and its derivatives (butyrylcarnitine,
404 hexadecenoylcarnitine, hexanoylcarnitine, octanoylcarnitine, and eicosanoyl carnitine)
405 from the carnitine shuttle, which is responsible for transferring long-chain fatty acids
406 across the inner mitochondrial membrane to access the beta-oxidation enzymes.
407 Moreover, this cluster includes energy sources such as DG compounds (DG(38:4),
408 DG(40:7), DG40:3), DG(38:7), etc.) and ADP and membrane-integrity-related
409 glycerophospholipids (PE(40:5), PE(34:1), PC(40:6, PS(32:0), and others), Figure 3a and
410 Supplementary Figure S5.

411 A second large cluster of annotated metabolites showed sorting-induced increases
412 in both comparisons. These metabolites include AMP (derived from ATP hydrolysis) and

propionyl carnitine (formed by the action of carnitine acetyltransferase during the β-oxidation of odd-numbered fatty acids), possibly reflecting the accumulation of energy consumption by-products. Sorting also upregulated a group of AA metabolites involved in LT synthesis. These metabolites derive from PUFAs that undergo series of oxidations through the action of COX and LOX. Since the lipid mediator precursors of these pathways are rapidly converted, it is likely that the two metabolites share similar activities. Upregulation of these annotated metabolites reflects activation of cell inflammatory responses. The second cluster also included several glycerophospholipids (LysoPE(24:6), PC(O-44:5), PC(36:4), PC(36:6)), sphingolipids, 2 ceramides (Cer(d40:2) and Cer(d46:0(2OH))/Cer(t46:0)), and a few short-chain and medium-chain fatty acids (4-oxo2-nonenal, 2-aminotridecanoic acid, 11-aminoundecanoic acid), Figure 3a and Supplementary Figure S5.

A total of 109 annotated metabolites were significantly altered only in the Ab+Sort group (Supplementary Figure S1g). This compound subset may reflect a synergistic effect of the immunostaining protocol and mechanical impact of the instrument on cell metabolism. Clustering analysis revealed that metabolites that were significantly decreased in Ab+Sort showed the same tendency in Sort, but with lower significance (Supplementary Figure S6). The decreased metabolite cluster in Ab+Sort included carnitine derivatives, DG compounds, fatty acids, and glycerophospholipids (Supplementary Figure S6). The Ab+Sort and Sort groups thus show a similarly severe downregulation of energy producing processes, but with the changes more pronounced in the Ab+Sort group (Supplementary Figure S6, FCs in Supplementary Table S3). Another cluster of annotated

435 metabolites was principally increased in the Ab+Sort group (top block in Supplementary
436 Figure S6). The subset of signalling lipid molecules in this cluster differs slightly to that
437 increased in Sort. This effect may reflect the binding of antibodies in the Ab+Sort group to
438 a type C tyrosine protein phosphatase receptor (PTPRC or CD45)); interaction of the
439 antibody-bound receptor with the cell membrane could cause additional stress and
440 enhance signalling activity in the vicinity of the membrane.

## CONCLUSIONS

Our results provide strong evidence that FACS analysis alters cell metabolism, triggering several phenomena linked to the physical stress cells undergo during sorting, inducing increased energy consumption and eventual cell damage that may also be related with the cellular starving caused by the resuspension of the cells in a pour nutrient media during the flow cytometry. The plasma membrane is the sole physical barrier separating cell components from the external environment and is an important reservoir of signalling molecules, mechanosensitive $Ca^{2+}$ channels, and other membrane receptors and receptor-coupled accessory proteins. During FACS, although the instrument-derived mechanical stimuli do not markedly compromise bilayer integrity, the cleavage of several membrane lipids is activated, triggering multiple stress-related pathways (Figure 5). Several of the altered biochemical pathways involve phospholipases activated in response to the mechanical stress exerted on the cell membrane. Translocation of mechanosensitive PLA2 to the cell membrane[20, 21] is trigged both by mechanical pressure and by increases in cellular $Ca^{2+}$, indicating tight interconnection between $Ca^{2+}$ signaling and AA metabolism. $Ca^{2+}$ is required for the enzymatic activation of the main PLA2 isoform. Cytosolic PLA2 associates with cell membranes in response to physiological $Ca^{2+}$ increases and selectively hydrolyses arachidonyl phospholipids[57].

Tension in the lipid bilayer plays a crucial role in sensory mechanotransduction and directly activates a series of eukaryotic calcium-permeable cell membrane channels, including members of the transient receptor potential (TRP) protein family[16-19]. Many TRP family $Ca^{2+}$ channels are activated by osmotonicity and stress through their ability to sense

fluid flow[58-63]. TRP channels are also directly activated by AA and its metabolites[64-67], completing the link between mechanical stimuli, AA signalling, and $Ca^{2+}$ signalling. Intracellular $Ca^{2+}$ concentrations increase upon modulation of mechanically gated membrane channels in response to physical stress, providing the necessary ion environment for PLA enzymatic activity[20, 68, 69].

All these pathways are linked to changes in cytosolic $Ca^{2+}$ concentration, produced by the activation of $Ca^{2+}$ membrane channels by the osmotonic and mechanical stress imposed during the passage of cells through the hydraulic system of the flow cytometer. Moreover, our data suggests that sorting induces Cer release from the SM reservoir. SM is an abundant constituent of the outer leaflet of the plasma membranes of mammalian cells[70]. SM hydrolysis by neutral SMase produces phosphocholine and Cer and has been suggested as a major route for stress-induced Cer production[71]. The sorting-induced changes in the SM and Cer pool thus might take place via the induction of plasma membrane-bound, $Mg^{2+}$-dependent, mechanosensitive SMase, which has been postulated as an intracellular promoter of apoptosis[51, 52] and has also been linked to the extracellular signal-regulated kinase 1 cascade and proinflammatory responses.

Our results highlight the need to include internal controls in FACS experiments to assess the impact of cell sorting on the cells being isolated. To minimize the impact of FACS influence on cell phenotype, control and experimental groups should undergo the same technical procedures, and particular attention should be paid to the technique-sensitive compounds identified here, especially when they form the focus of the research.

## ASSOCIATED CONTENT

## SUPPORTING INFORMATION:

The following supporting information is available free of charge at ACS website http://pubs.acs.org

Supplementary Table S1 Metabolite extraction parameters. (PDF)

Supplementary Table S2. Number of metabolic features (raw or annotated compounds), with an explanation after each workflow step. (PDF)

Supplementary Table S3. Compounds showing statistically significant FACS-induced abundance changes, together with their annotated identifications. (XLSX)

Supplementary Figure S1. Principal component analysis (PCA) plots showing the effects on the metabolome of immunostaining and flow cytometry. (PDF)

Supplementary Figure S2. Venn diagrams representing co-detected metabolites. (PDF)

Supplementary Figure S3. Box plots of cross-platform validation (all metabolites were identified in 2 or more analytical approaches). (PDF)

Supplementary Figure S4. Impact on metabolic pathways in sorted mouse peritoneal macrophages. (PDF)

Supplementary Figure S5. Hierarchical clustering analysis of annotated metabolites significantly altered in both the Sort and Ab+Sort groups. (PDF)

Supplementary Figure S6. Hierarchical clustering analysis of annotated metabolites significantly altered only in the Ab+Sort group. (PDF)

Supplementary Figure S7. FACS analysis of the peritoneal macrophage population isolated from thioglycollate-injected BLC6 mice was performed with 5 biological replicates. (PDF)

## AUTHOR INFORMATION

### Corresponding Author

* Correspondence and requests for materials should be addressed to:

Coral Barbas (cbarbas@ceu.es)

Centro de Metabolómica y Bioanálisis (CEMBIO), Facultad de Farmacia

Universidad CEU San Pablo, Campus Montepríncipe

Boadilla del Monte

28668 Madrid, Spain

### Author contributions

The manuscript was written through contributions of all authors. All authors have given approval to the final version of the manuscript. A.B. and D.R. performed the metabolome analysis, interpreted data, and prepared the manuscript. C.B. and FJ.R. helped with manuscript preparation and funding acquisition, and provided analytical and intellectual input on the metabolome data. J.G. helped with metabolite identification. A.B. and V.N.

prepared the macrophage samples. J.V., M.R. and I.J. helped with the experimental design.

## Funding sources

C.B., FJ.R., J.G., and D.R. acknowledge funding from the Ministerio de Economía y Competitividad (CTQ2014-55279-R). This study was also supported by Ministerio de Economía y Competitividad grant BIO2015-67580-P through the Carlos III Institute of Health (ISCIII) and the Fundación La Marató TV3 to J.V and to M.R (201605-30-31-32). J.V. laboratory is a member of Proteored, PRB3 and is supported by grant PT17/0019, of the PE I+D+i 2013-2016, funded by ISCIII and European Regional Development Fund (ERDF). M.R. received grants from the Ministerio de Economía y Competitividad (SAF2015-64287R, SAF2017-90604-REDT). J.V and M.R received funding from the People Programme (Marie Curie Actions) of the European Union Seventh Framework Programme (FP7/2007-2013) under REA grant agreement nº 608027 (CardioNext Initial Training Networks project). A.B. is a FP7-PEOPLE-2013-ITN-Cardionext fellow. The CNIC is supported by the Ministerio de Ciencia, Innovación y Universidades (MCNU) and the Pro-CNIC Foundation, and is a Severo Ochoa Center of Excellence (SEV-2015-0505).

## ACKNOWLEDGMENT

A.B. and D.R. acknowledge Fernanda Rey-Stolle for intellectual input on GC-MS data treatment. Simon Bartlett (CNIC) provided English editing. Graphical elements in Figure 1 and 5 as well as in the graphical abstract were adapted from the Servier Medical Art (SMART) PowerPoint image bank. SMART by Servier (https://smart.servier.com/) is

ABBREVIATIONS

FCs, fold changes; FACS, fluorescence-activated cell sorting; MS, mass spectrometry; LC, liquid chromatography; CE, capillary electrophoresis; GC, and gas chromatography; PLA2, phospholipase A2; QCs, quality controls; PCA, principal component analysis; HMDB, Human Metabolome Database; AA, arachidonic acid; COX, cyclooxygenase; PGs, prostaglandins; LOX, lipoxygenase; LTs, leukotrienes; LA, linoleic acid; PUFAs, polyunsaturated fatty acids; EPA, eicosapentaenoic acid; DHA, docosahexaenoic acid; LysoPC, lysophospholipids; LPL, lysophospholipase; PLC and PLD, phospholipase C and D; DG, diacyglycerols; PA, phosphatidic acids; 2-AG, 2-arachidonoylglycerol; AEA, anandamide (20:4, n=6); EPEA, anandamide (20:5, n=3); PC, phosphatidylcholine; PI, phosphatidylinositol; PE, phosphatidylethanolamine; SM, sphingomyelins; Cer, ceramides; CEHC, carboxy-ethyl-hydroxy-chroman; PTPRC, type C tyrosine protein phosphatase receptor; TRP, transient receptor potential protein family.

**COMPETING FINANCIAL INTERESTS**

The authors declare no competing financial interests.

## REFERENCES


1. Fan, Y.; Hanai, J. I.; Le, P. T.; Bi, R.; Maridas, D.; DeMambro, V.; Figueroa, C. A.; Kir, S.; Zhou, X.; Mannstadt, M.; Baron, R.; Bronson, R. T.; Horowitz, M. C.; Wu, J. Y.; Bilezikian, J. P.; Dempster, D. W.; Rosen, C. J.; Lanske, B., Parathyroid Hormone Directs Bone Marrow Mesenchymal Cell Fate. *Cell Metab* **2017,** 25, (3), 661-672.
2. Wenes, M.; Shang, M.; Di Matteo, M.; Goveia, J.; Martin-Perez, R.; Serneels, J.; Prenen, H.; Ghesquiere, B.; Carmeliet, P.; Mazzone, M., Macrophage Metabolism Controls Tumor Blood Vessel Morphogenesis and Metastasis. *Cell Metab* **2016,** 24, (5), 701-715.
3. Hirth, M.; Liverani, S.; Mahlow, S.; Bouget, F. Y.; Pohnert, G.; Sasso, S., Metabolic profiling identifies trehalose as an abundant and diurnally fluctuating metabolite in the microalga Ostreococcus tauri. *Metabolomics* **2017,** 13, (6), 68.
4. Sukumar, M.; Liu, J.; Mehta, G. U.; Patel, S. J.; Roychoudhuri, R.; Crompton, J. G.; Klebanoff, C. A.; Ji, Y.; Li, P.; Yu, Z.; Whitehill, G. D.; Clever, D.; Eil, R. L.; Palmer, D. C.; Mitra, S.; Rao, M.; Keyvanfar, K.; Schrump, D. S.; Wang, E.; Marincola, F. M.; Gattinoni, L.; Leonard, W. J.; Muranski, P.; Finkel, T.; Restifo, N. P., Mitochondrial Membrane Potential Identifies Cells with Enhanced Stemness for Cellular Therapy. *Cell Metab* **2016,** 23, (1), 63-76.
5. Ying, Q. L.; Stavridis, M.; Griffiths, D.; Li, M.; Smith, A., Conversion of embryonic stem cells into neuroectodermal precursors in adherent monoculture. *Nat Biotechnol* **2003,** 21, (2), 183-6.
6. Claudi, B.; Sprote, P.; Chirkova, A.; Personnic, N.; Zankl, J.; Schurmann, N.; Schmidt, A.; Bumann, D., Phenotypic variation of Salmonella in host tissues delays eradication by antimicrobial chemotherapy. *Cell* **2014,** 158, (4), 722-33.
7. Pechhold, S.; Stouffer, M.; Walker, G.; Martel, R.; Seligmann, B.; Hang, Y.; Stein, R.; Harlan, D. M.; Pechhold, K., Transcriptional analysis of intracytoplasmically stained, FACS-purified cells by high-throughput, quantitative nuclease protection. *Nat Biotechnol* **2009,** 27, (11), 1038-42.
8. Julius, M. H.; Masuda, T.; Herzenberg, L. A., Demonstration that antigen-binding cells are precursors of antibody-producing cells after purification with a fluorescence-activated cell sorter. *Proc Natl Acad Sci U S A* **1972,** 69, (7), 1934-8.
9. Moussaieff, A.; Rogachev, I.; Brodsky, L.; Malitsky, S.; Toal, T. W.; Belcher, H.; Yativ, M.; Brady, S. M.; Benfey, P. N.; Aharoni, A., High-resolution metabolic mapping of cell types in plant roots. *Proceedings of the National Academy of Sciences of the United States of America* **2013,** 110, (13), E1232-41.
10. Pencik, A.; Simonovik, B.; Petersson, S. V.; Henykova, E.; Simon, S.; Greenham, K.; Zhang, Y.; Kowalczyk, M.; Estelle, M.; Zazimalova, E.; Novak, O.; Sandberg, G.; Ljung, K., Regulation of auxin homeostasis and gradients in Arabidopsis roots through the formation of the indole-3-acetic acid catabolite 2-oxindole-3-acetic acid. *Plant Cell* **2013,** 25, (10), 3858-70.
11. Petersson, S. V.; Johansson, A. I.; Kowalczyk, M.; Makoveychuk, A.; Wang, J. Y.; Moritz, T.; Grebe, M.; Benfey, P. N.; Sandberg, G.; Ljung, K., An auxin gradient and maximum in the Arabidopsis root apex shown by high-resolution cell-specific analysis of IAA distribution and synthesis. *Plant Cell* **2009,** 21, (6), 1659-68.
12. Petersson, S. V.; Linden, P.; Moritz, T.; Ljung, K., Cell-type specific metabolic profiling of Arabidopsis thaliana protoplasts as a tool for plant systems biology. *Metabolomics* **2015,** 11, (6), 1679-1689.
13. Roci, I.; Gallart-Ayala, H.; Schmidt, A.; Watrous, J.; Jain, M.; Wheelock, C. E.; Nilsson, R., Metabolite Profiling and Stable Isotope Tracing in Sorted Subpopulations of Mammalian Cells. *Analytical chemistry* **2016,** 88, (5), 2707-13.
14. Llufrio, E. M.; Wang, L.; Naser, F. J.; Patti, G. J., Sorting cells alters their redox state and cellular metabolome. *Redox Biol* **2018,** 16, 381-387.

15. Fiehn, O.; Robertson, D.; Griffin, J.; van der Werf, M.; Nikolau, B.; Morrison, N.; Sumner, L. W.; Goodacre, R.; Hardy, N. W.; Taylor, C., The metabolomics standards initiative (MSI). *Metabolomics* **2007,** 3, (3), 175-178.
16. Kung, C., A possible unifying principle for mechanosensation. *Nature* **2005,** 436, (7051), 647-654.
17. Damann, N.; Voets, T.; Nilius, B., TRPs in Our Senses. *Current Biology* **2008,** 18, (18), R880-R889.
18. Myers, B. R.; Saimi, Y.; Julius, D.; Kung, C., Multiple Unbiased Prospective Screens Identify TRP Channels and Their Conserved Gating Elements. *The Journal of General Physiology* **2008,** 132, (5), 481-486.
19. Yin, J.; Kuebler, W. M., Mechanotransduction by TRP Channels: General Concepts and Specific Role in the Vasculature. *Cell Biochemistry and Biophysics* **2009,** 56, (1), 1.
20. van Rossum, D. B.; Patterson, R. L., PKC and PLA2: Probing the complexities of the calcium network. *Cell Calcium* **2009,** 45, (6), 535-545.
21. Lehtonen, J. Y.; Kinnunen, P. K., Phospholipase A2 as a mechanosensor. *Biophysical Journal* **1995,** 68, (5), 1888-1894.
22. Peterson, J. W.; Boldogh, I.; Popov, V. L.; Saini, S. S.; Chopra, A. K., Anti-inflammatory and antisecretory potential of histidine in Salmonella-challenged mouse small intestine. *Lab Invest* **1998,** 78, (5), 523-34.
23. Lisec, J.; Schauer, N.; Kopka, J.; Willmitzer, L.; Fernie, A. R., Gas chromatography mass spectrometry-based metabolite profiling in plants. *Nat Protoc* **2006,** 1, (1), 387-96.
24. Yuan, M.; Breitkopf, S. B.; Yang, X.; Asara, J. M., A positive/negative ion-switching, targeted mass spectrometry-based metabolomics platform for bodily fluids, cells, and fresh and fixed tissue. *Nat Protoc* **2012,** 7, (5), 872-81.
25. Rojo, D.; Canuto, G. A.; Castilho-Martins, E. A.; Tavares, M. F.; Barbas, C.; Lopez-Gonzalvez, A.; Rivas, L., A Multiplatform Metabolomic Approach to the Basis of Antimonial Action and Resistance in Leishmania infantum. *PLoS One* **2015,** 10, (7), e0130675.
26. Bargiela, R.; Mapelli, F.; Rojo, D.; Chouaia, B.; Tornes, J.; Borin, S.; Richter, M.; Del Pozo, M. V.; Cappello, S.; Gertler, C.; Genovese, M.; Denaro, R.; Martinez-Martinez, M.; Fodelianakis, S.; Amer, R. A.; Bigazzi, D.; Han, X.; Chen, J.; Chernikova, T. N.; Golyshina, O. V.; Mahjoubi, M.; Jaouanil, A.; Benzha, F.; Magagnini, M.; Hussein, E.; Al-Horani, F.; Cherif, A.; Blaghen, M.; Abdel-Fattah, Y. R.; Kalogerakis, N.; Barbas, C.; Malkawi, H. I.; Golyshin, P. N.; Yakimov, M. M.; Daffonchio, D.; Ferrer, M., Bacterial population and biodegradation potential in chronically crude oil-contaminated marine sediments are strongly linked to temperature. *Sci Rep* **2015,** 5, 11651.
27. Whiley, L.; Godzien, J.; Ruperez, F. J.; Legido-Quigley, C.; Barbas, C., In-vial dual extraction for direct LC-MS analysis of plasma for comprehensive and highly reproducible metabolic fingerprinting. *Anal Chem* **2012,** 84, (14), 5992-9.
28. Kind, T.; Wohlgemuth, G.; Lee, d. Y.; Lu, Y.; Palazoglu, M.; Shahbaz, S.; Fiehn, O., FiehnLib: mass spectral and retention index libraries for metabolomics based on quadrupole and time-of-flight gas chromatography/mass spectrometry. *Anal Chem* **2009,** 81, (24), 10038-48.
29. Godzien, J.; Alonso-Herranz, V.; Barbas, C.; Armitage, E. G., Controlling the quality of metabolomics data: new strategies to get the best out of the QC sample. *Metabolomics* **2014,** 11, (3), 518-528.
30. Armitage, E. G.; Godzien, J.; Alonso-Herranz, V.; López-Gonzálvez, Á.; Barbas, C., Missing value imputation strategies for metabolomics data. *Electrophoresis* **2015,** 36, (24), 3050-60.
31. Godzien, J.; Ciborowski, M.; Armitage, E. G.; Jorge, I.; Camafeita, E.; Burillo, E.; Martín-Ventura, J. L.; Rupérez, F. J.; Vázquez, J.; Barbas, C., A Single In-Vial Dual Extraction Strategy for the

653 Simultaneous Lipidomics and Proteomics Analysis of HDL and LDL Fractions. *J Proteome Res* **2016,**
654 15, (6), 1762-1775.
655 32. Godzien, J.; Ciborowski, M.; Martinez-Alcazar, M. P.; Samczuk, P.; Kretowski, A.; Barbas, C.,
656 Rapid and Reliable Identification of Phospholipids for Untargeted Metabolomics with LC-ESI-QTOF-
657 MS/MS. *Journal of proteome research* **2015,** 14, (8), 3204-16.
658 33. Godzien, J.; Armitage, E. G.; Angulo, S.; Martinez-Alcazar, M. P.; Alonso-Herranz, V.; Otero,
659 A.; Lopez-Gonzalvez, A.; Barbas, C., In-source fragmentation and correlation analysis as tools for
660 metabolite identification exemplified with CE-TOF untargeted metabolomics. *Electrophoresis*
661 **2015,** 36, (18), 2188-2195.
662 34. Salek, R. M.; Steinbeck, C.; Viant, M. R.; Goodacre, R.; Dunn, W. B., The role of reporting
663 standards for metabolite annotation and identification in metabolomic studies. *Gigascience* **2013,**
664 2, (1), 13.
665 35. Xia, J.; Sinelnikov, I. V.; Han, B.; Wishart, D. S., MetaboAnalyst 3.0--making metabolomics
666 more meaningful. *Nucleic Acids Res* **2015,** 43, (W1), W251-7.
667 36. Armitage, E. G.; Godzien, J.; Pena, I.; Lopez-Gonzalvez, A.; Angulo, S.; Gradillas, A.; Alonso-
668 Herranz, V.; Martin, J.; Fiandor, J. M.; Barrett, M. P.; Gabarro, R.; Barbas, C., Metabolic Clustering
669 Analysis as a Strategy for Compound Selection in the Drug Discovery Pipeline for Leishmaniasis.
670 *ACS Chem Biol* **2018,** 13, (5), 1361-1369.
671 37. Patwardhan, A. M.; Scotland, P. E.; Akopian, A. N.; Hargreaves, K. M., Activation of TRPV1
672 in the spinal cord by oxidized linoleic acid metabolites contributes to inflammatory hyperalgesia.
673 *Proceedings of the National Academy of Sciences of the United States of America* **2009,** 106, (44),
674 18820-18824.
675 38. Murakami, M., Lipid mediators in life science. *Exp Anim* **2011,** 60, (1), 7-20.
676 39. Arduin, A.; Gaffney, P. R.; Ces, O., Regulation of PLCbeta2 by the electrostatic and
677 mechanical properties of lipid bilayers. *Sci Rep* **2015,** 5, 12628.
678 40. Gao, G.; He, J.; Nong, L.; Xie, H.; Huang, Y.; Xu, N.; Zhou, D., Periodic mechanical stress
679 induces the extracellular matrix expression and migration of rat nucleus pulposus cells by
680 upregulating the expression of intergrin alpha1 and phosphorylation of downstream
681 phospholipase Cgamma1. *Mol Med Rep* **2016,** 14, (3), 2457-64.
682 41. Ren, K.; Ma, Y.; Huang, Y.; Liang, W.; Liu, F.; Wang, Q.; Cui, W.; Liu, Z.; Yin, G.; Fan, W.,
683 Periodic mechanical stress activates MEK1/2-ERK1/2 mitogenic signals in rat chondrocytes through
684 Src and PLCgamma1. *Braz J Med Biol Res* **2011,** 44, (12), 1231-42.
685 42. Bisogno, T.; Howell, F.; Williams, G.; Minassi, A.; Cascio, M. G.; Ligresti, A.; Matias, I.;
686 Schiano-Moriello, A.; Paul, P.; Williams, E.-J.; Gangadharan, U.; Hobbs, C.; Di Marzo, V.; Doherty,
687 P., Cloning of the first sn1-DAG lipases points to the spatial and temporal regulation of
688 endocannabinoid signaling in the brain. *The Journal of Cell Biology* **2003,** 163, (3), 463-468.
689 43. Reisenberg, M.; Singh, P. K.; Williams, G.; Doherty, P., The diacylglycerol lipases: structure,
690 regulation and roles in and beyond endocannabinoid signalling. *Philosophical Transactions of the*
691 *Royal Society B: Biological Sciences* **2012,** 367, (1607), 3264-3275.
692 44. Balgoma, D.; Astudillo, A. M.; Pérez-Chacón, G.; Montero, O.; Balboa, M. A.; Balsinde, J.,
693 Markers of Monocyte Activation Revealed by Lipidomic Profiling of Arachidonic Acid-Containing
694 Phospholipids. *The Journal of Immunology* **2010,** 184, (7), 3857-3865.
695 45. Shamsuddin, A. K. M.; Yang, G.-Y., *Inositol & its Phosphates: Basic Science to Practical*
696 *Applications*. Bentham Science Publishers Ltd: Sharjah, 2015; p 16-23.
697 46. Petrache, H. I.; Tristram-Nagle, S.; Gawrisch, K.; Harries, D.; Parsegian, V. A.; Nagle, J. F.,
698 Structure and Fluctuations of Charged Phosphatidylserine Bilayers in the Absence of Salt.
699 *Biophysical Journal* **2004,** 86, (3), 1574-1586.

47. Verhoven, B.; Schlegel, R. A.; Williamson, P., Mechanisms of phosphatidylserine exposure, a phagocyte recognition signal, on apoptotic T lymphocytes. *The Journal of Experimental Medicine* **1995,** 182, (5), 1597-1601.
48. Yu, R. K.; Tsai, Y.-T.; Ariga, T.; Yanagisawa, M., Structures, biosynthesis, and functions of gangliosides—An overview. *Journal of oleo science* **2011,** 60, (10), 537-544.
49. Czarny, M.; Liu, J.; Oh, P.; Schnitzer, J. E., Transient mechanoactivation of neutral sphingomyelinase in caveolae to generate ceramide. *J Biol Chem* **2003,** 278, (7), 4424-30.
50. Czarny, M.; Schnitzer, J. E., Neutral sphingomyelinase inhibitor scyphostatin prevents and ceramide mimics mechanotransduction in vascular endothelium. *Am J Physiol Heart Circ Physiol* **2004,** 287, (3), H1344-52.
51. Tomiuk, S.; Hofmann, K.; Nix, M.; Zumbansen, M.; Stoffel, W., Cloned mammalian neutral sphingomyelinase: Functions in sphingolipid signaling? *Proceedings of the National Academy of Sciences of the United States of America* **1998,** 95, (7), 3638-3643.
52. Zhang, Y.; Yao, B.; Delikat, S.; Bayoumy, S.; Lin, X. H.; Basu, S.; McGinley, M.; Chan-Hui, P. Y.; Lichenstein, H.; Kolesnick, R., Kinase suppressor of Ras is ceramide-activated protein kinase. *Cell* **1997,** 89, (1), 63-72.
53. Park, M.-T.; Kang, J. A.; Choi, J.-A.; Kang, C.-M.; Kim, T.-H.; Bae, S.; Kang, S.; Kim, S.; Choi, W.-I.; Cho, C.-K.; Chung, H.-Y.; Lee, Y.-S.; Lee, S.-J., Phytosphingosine Induces Apoptotic Cell Death via Caspase 8 Activation and Bax Translocation in Human Cancer Cells. *Clinical Cancer Research* **2003,** 9, (2), 878-885.
54. Schreiber, V.; Dantzer, F.; Ame, J. C.; de Murcia, G., Poly(ADP-ribose): novel functions for an old molecule. *Nat Rev Mol Cell Biol* **2006,** 7, (7), 517-28.
55. Krajewski, W. A., Effect of Nonenzymatic Histone Acetylation on Chromatin High-Order Folding. *Biochem Biophys Res Commun* **1996,** 221, (2), 295-299.
56. Son, D. O.; Satsu, H.; Shimizu, M., Histidine inhibits oxidative stress- and TNF-α-induced interleukin-8 secretion in intestinal epithelial cells. *FEBS Letters* **2005,** 579, (21), 4671-4677.
57. Lee, K. S.; Patton, J. L.; Fido, M.; Hines, L. K.; Kohlwein, S. D.; Paltauf, F.; Henry, S. A.; Levin, D. E., The Saccharomyces cerevisiae PLB1 gene encodes a protein required for lysophospholipase and phospholipase B activity. *J Biol Chem* **1994,** 269, (31), 19725-30.
58. Watanabe, H.; Vriens, J.; Prenen, J.; Droogmans, G.; Voets, T.; Nilius, B., Anandamide and arachidonic acid use epoxyeicosatrienoic acids to activate TRPV4 channels. *Nature* **2003,** 424, (6947), 434-8.
59. Vriens, J.; Watanabe, H.; Janssens, A.; Droogmans, G.; Voets, T.; Nilius, B., Cell swelling, heat, and chemical agonists use distinct pathways for the activation of the cation channel TRPV4. *Proceedings of the National Academy of Sciences of the United States of America* **2004,** 101, (1), 396-401.
60. Nilius, B.; Vriens, J.; Prenen, J.; Droogmans, G.; Voets, T., TRPV4 calcium entry channel: a paradigm for gating diversity. *Am J Physiol Cell Physiol* **2004,** 286, (2), C195-205.
61. Nilius, B.; Watanabe, H.; Vriens, J., The TRPV4 channel: structure-function relationship and promiscuous gating behaviour. *Pflugers Arch* **2003,** 446, (3), 298-303.
62. Vriens, J.; Owsianik, G.; Fisslthaler, B.; Suzuki, M.; Janssens, A.; Voets, T.; Morisseau, C.; Hammock, B. D.; Fleming, I.; Busse, R.; Nilius, B., Modulation of the Ca2 permeable cation channel TRPV4 by cytochrome P450 epoxygenases in vascular endothelium. *Circ Res* **2005,** 97, (9), 908-15.
63. Sharif-Naeini, R.; Folgering, J. H.; Bichet, D.; Duprat, F.; Lauritzen, I.; Arhatte, M.; Jodar, M.; Dedman, A.; Chatelain, F. C.; Schulte, U.; Retailleau, K.; Loufrani, L.; Patel, A.; Sachs, F.; Delmas, P.; Peters, D. J.; Honore, E., Polycystin-1 and -2 dosage regulates pressure sensing. *Cell* **2009,** 139, (3), 587-96.

64. Hardie, R. C., TRP channels and lipids: from Drosophila to mammalian physiology. *J Physiol* **2007,** 578, (Pt 1), 9-24.
65. Hardie, R. C., Regulation of TRP channels via lipid second messengers. *Annu Rev Physiol* **2003,** 65, 735-59.
66. Hardie, R. C.; Muallem, S., Lipids in Ca2+ signalling--an introduction. *Cell Calcium* **2009,** 45, (6), 517-20.
67. Hofmann, T.; Obukhov, A. G.; Schaefer, M.; Harteneck, C.; Gudermann, T.; Schultz, G., Direct activation of human TRPC6 and TRPC3 channels by diacylglycerol. *Nature* **1999,** 397, (6716), 259-63.
68. Burke, J. E.; Dennis, E. A., Phospholipase A2 structure/function, mechanism, and signaling. *J Lipid Res* **2009,** 50 Suppl, S237-42.
69. Lambert, I. H.; Pedersen, S. F.; Poulsen, K. A., Activation of PLA2 isoforms by cell swelling and ischaemia/hypoxia. *Acta Physiol (Oxf)* **2006,** 187, (1-2), 75-85.
70. Slotte, J. P.; Härmälä, A.-S.; Jansson, C.; Pörn, M. I., Rapid turn-over of plasma membrane sphingomyelin and cholesterol in baby hamster kidney cells after exposure to sphingomyelinase. *Biochimica et Biophysica Acta (BBA) - Biomembranes* **1990,** 1030, (2), 251-257.
71. Hannun, Y. A.; Obeid, L. M., The Ceramide-centric Universe of Lipid-mediated Cell Regulation: Stress Encounters of the Lipid Kind. *Journal of Biological Chemistry* **2002,** 277, (29), 25847-25850.

770 **FIGURE LEGENDS**

771 **Figure 1**. Simplified workflow for the metabolomic study of FACS-sorted peritoneal
772 macrophages. C57BL/6 mice received thioglycollate injections in the peritoneal cavity, and
773 macrophages were collected after 72 h. Cells were counted under a microscope and
774 divided in to 4 equal samples. The cell pellet of the Ctrl experimental group was snap-
775 frozen immediately after isolation. Cells in the Ab samples were resuspended in blocking
776 buffer and incubated with anti-CD16/CD32 and PerCP-Cy5.5-labeled anti-CD45, followed
777 by washing and snap-freezing in liquid N2. The Sort and Ab+Sort samples were prepared
778 according to the protocols for the Ctrl and Ab groups, respectively, but before the final
779 snap-freezing step the cells these 2 experimental groups were subjected to flow
780 cytometry. Metabolites were extracted from all cell pellets with i) MTBE:MetOH and ii)
781 MetOH:H2O, and the resulting supernatants were analysed by GC-EI-QMS, CE-ESI-TOF-MS,
782 and LC-ESI-QTOF-MS in positive and negative ionization modes in 2 chromatographic
783 gradients (general and lipid). Five biological replicates were injected. Quality control (QC)
784 samples were prepared by pooling equal volumes of all metabolite extracts and injected in
785 between blocks of 4 samples until the end of the run to ensure analytical reproducibility.
786 Image courtesy of Servier Medical Art (SMART) PowerPoint image bank
787 (https://smart.servier.com/).

788

789 **Figure 2.** Selected boxplots representing the intensity of annotated metabolites (inosine
790 monophosphate, phenylalanine, linoleyl carnitine, hypoxanthine, alpha-CEHC, histidine,
791 creatine, and LysoPE(20:0)) codetected by different separation techniques. These

metabolites were selected to illustrate distinct analytical situations and biochemical classes. The selection covers downregulated metabolites involved in pathways of energy generation, storage, and transfer (creatine, linoleyl carnitine), structural compounds (lysophospholipids), nucleic acid metabolism (hypoxanthine, IMP), and others (alpha-CEHC, histidine). Results are shown as box and whisker plots of minimum to maximum values obtained in 5 replicates. * Indicates p value $< 0.05$ versus baseline by Mann-Whitney U test followed by Benjamini-Hochberg post hoc correction.

**Figure 3.** Biochemical classes altered in 3 experimental conditions with respect to the control group (Ctrl): Ab, Sort, and Ab+Sort. (**a**) Hierarchical clustering analysis of metabolites showing statistically significant alteration. (**b**) Direction of changes in the subpopulations of amino acids, peptides, and analogues. (**c**) Biochemical categories (sub-class in HMDB) of metabolites showing statistically significant alteration (Mann-Whitney U test followed by Benjamini-Hochberg post hoc correction, p value $< 0.05$, n=5) with manually curated identification. For details see Supplementary Figure S5 and Supplementary Table S3.

**Figure 4**.

The heatmap represents the $\log_2$ fold changes of individual samples intensities in each condition with respect to Ctrl sample average intensity. Selected groups of metabolites with manually curated identification show statistically significant alterations (Benjamini-

813 Hochberg post hoc correction, p value < 0.05 in bold italics). For further details such as
814 individual intensities or separation techniques see Supplementary Table S3.
815
816 **Figure 5.** FACS affects cell metabolism. The figure represents some of the main stress
817 inputs, including a graphical summary of the mechanosensitive cascade triggered by
818 mechanical stimulus of the plasma membrane (inset). Image courtesy of Servier Medical
819 Art (SMART) PowerPoint image bank (https://smart.servier.com/).
820
821
822
823

**FIGURES**

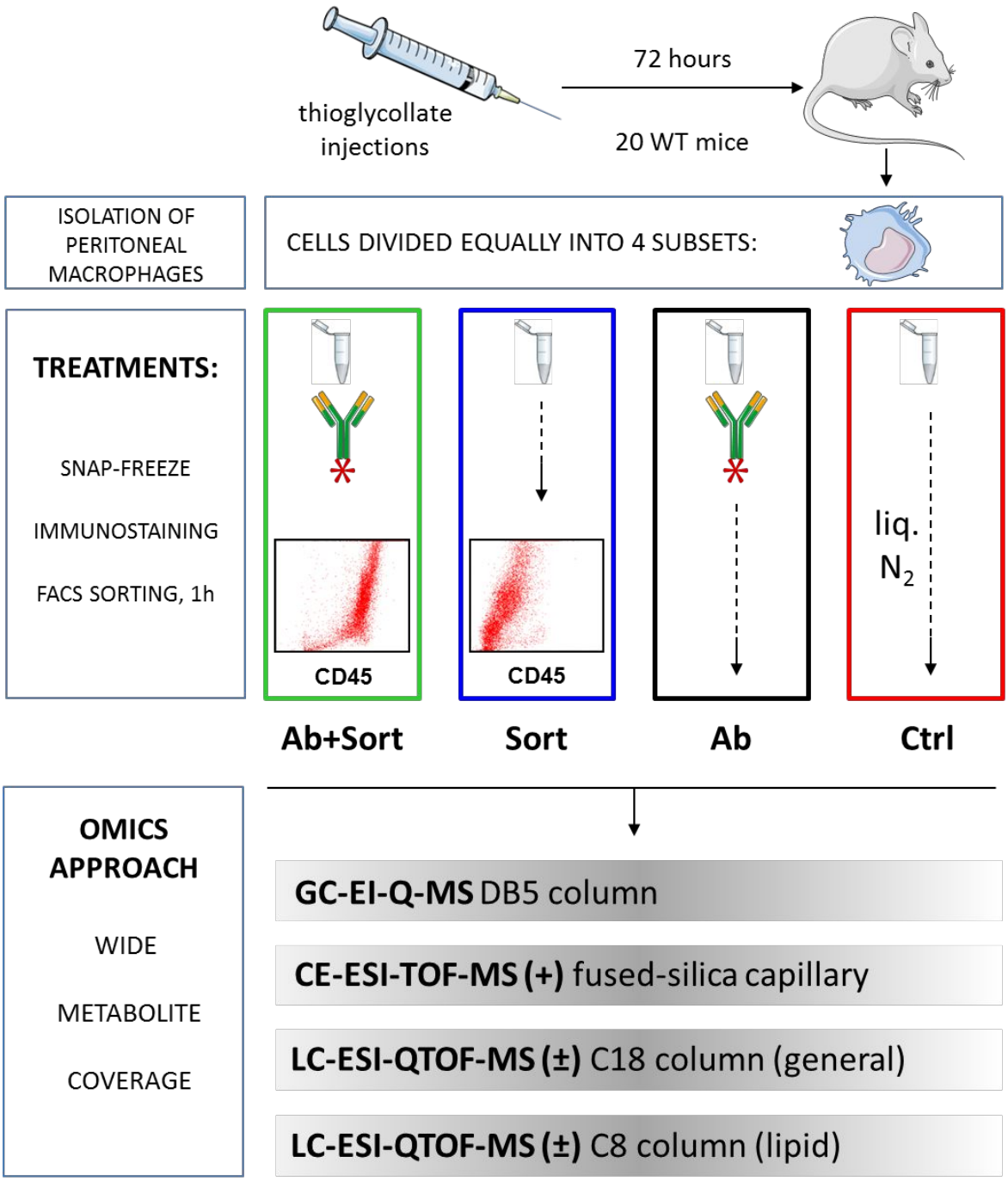


**Figure 1.**

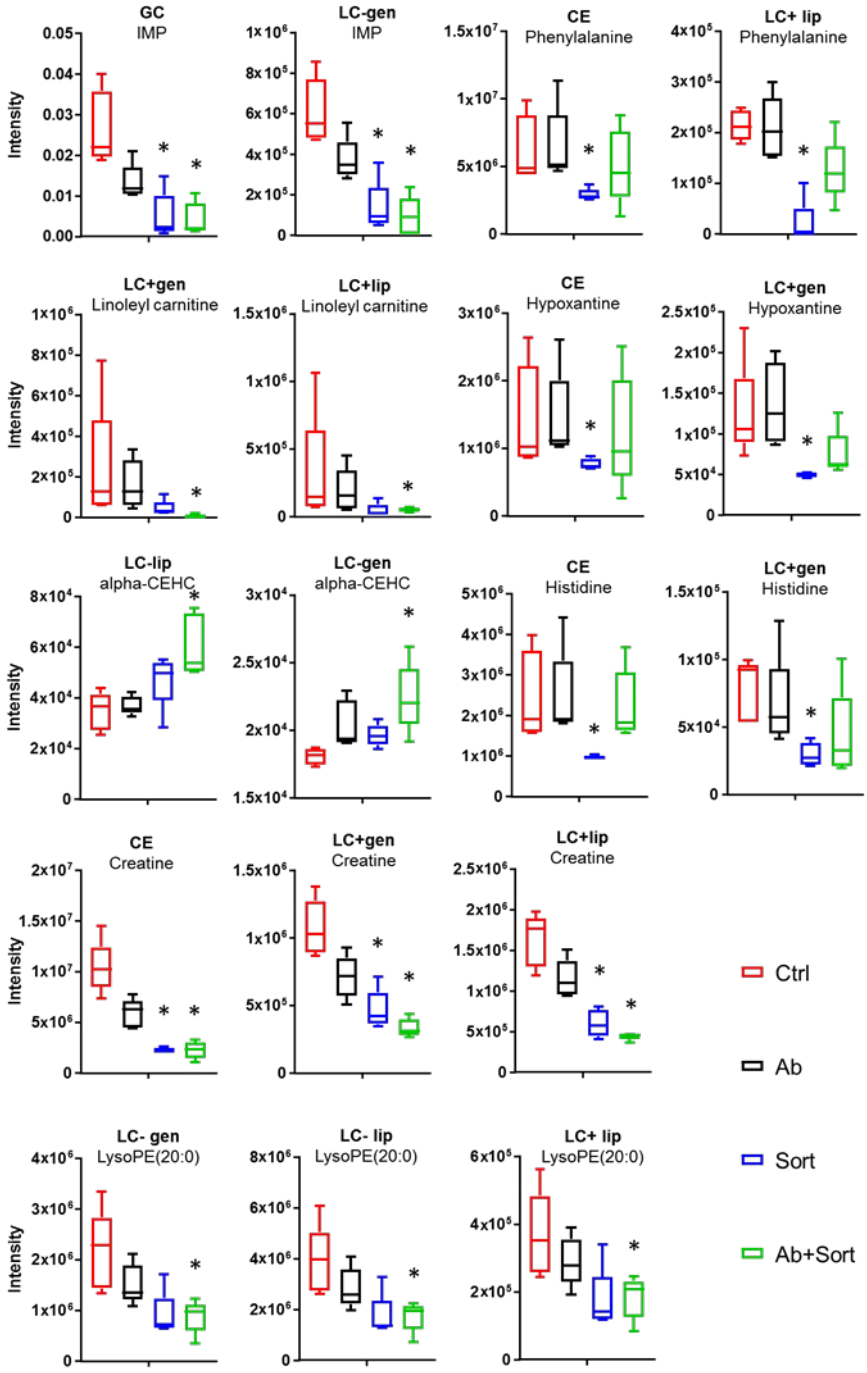
GC
IMP
LC-gen
IMP
CE
Phenylalanine
LC+ lip
Phenylalanine
LC+gen
Linoleyl carnitine
LC+lip
Linoleyl carnitine
CE
Hypoxantine
LC+gen
Hypoxantine
LC-lip
alpha-CEHC
LC-gen
alpha-CEHC
CE
Histidine
LC+gen
Histidine
CE
Creatine
LC+gen
Creatine
LC+lip
Creatine
LC- gen
LysoPE(20:0)
LC- lip
LysoPE(20:0)
LC+ lip
LysoPE(20:0)
Intensity
Ctrl
Ab
Sort
Ab+Sort

**Figure 2**.

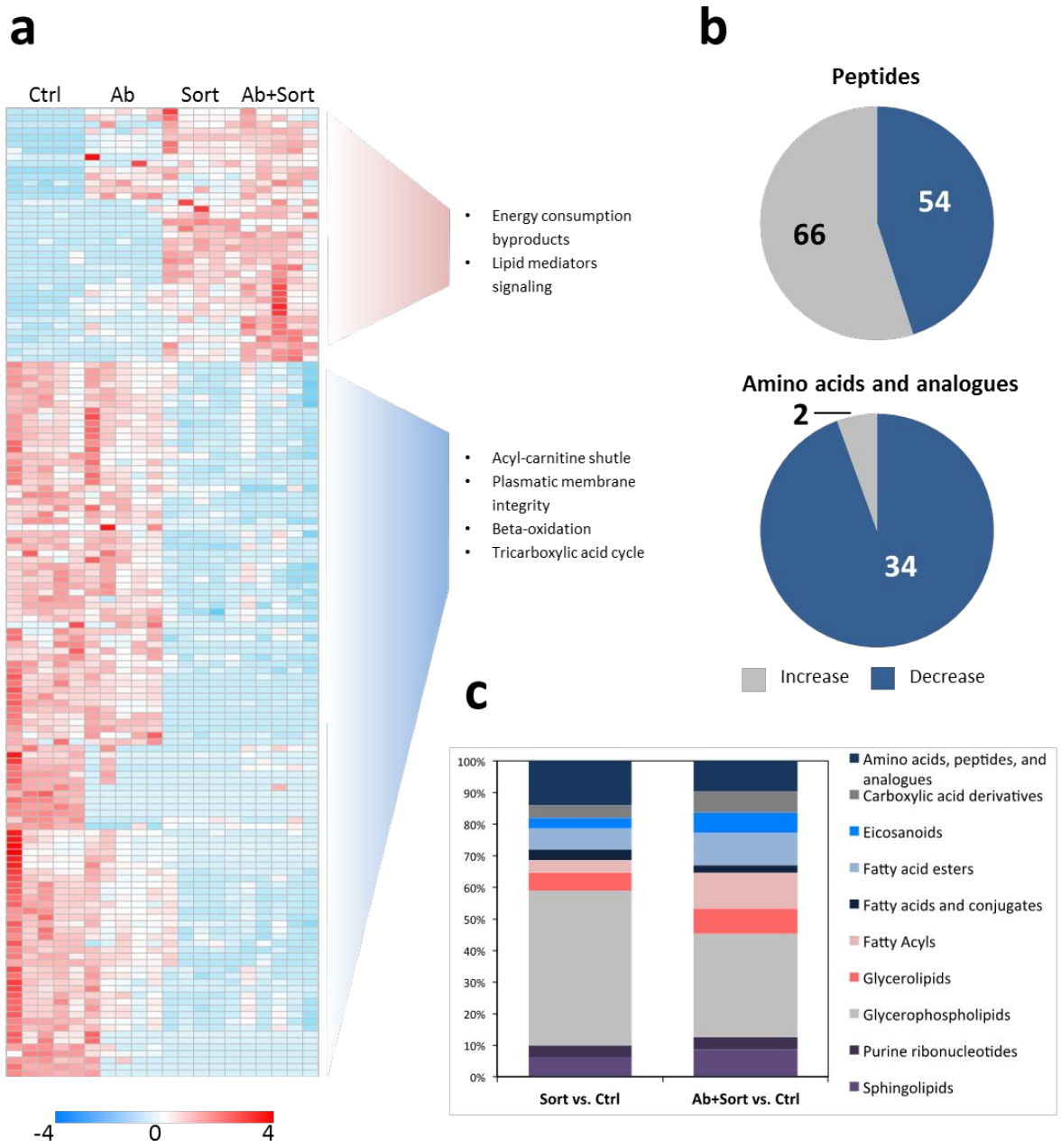
a
Ctrl
Ab
Sort
Ab+Sort
-4
0
4
Energy consumption byproducts
Lipid mediators signaling
Acyl-carnitine shutle
Plasmatic membrane integrity
Beta-oxidation
Tricarboxylic acid cycle
b
Peptides
54
66
Amino acids and analogues
2
34
Increase
Decrease
c
100%
90%
80%
70%
60%
50%
40%
30%
20%
10%
0%
Sort vs. Ctrl
Ab+Sort vs. Ctrl
Amino acids, peptides, and analogues
Carboxylic acid derivatives
Eicosanoids
Fatty acid esters
Fatty acids and conjugates
Fatty Acyls
Glycerolipids
Glycerophospholipids
Purine ribonucleotides
Sphingolipids

**Figure 3.**

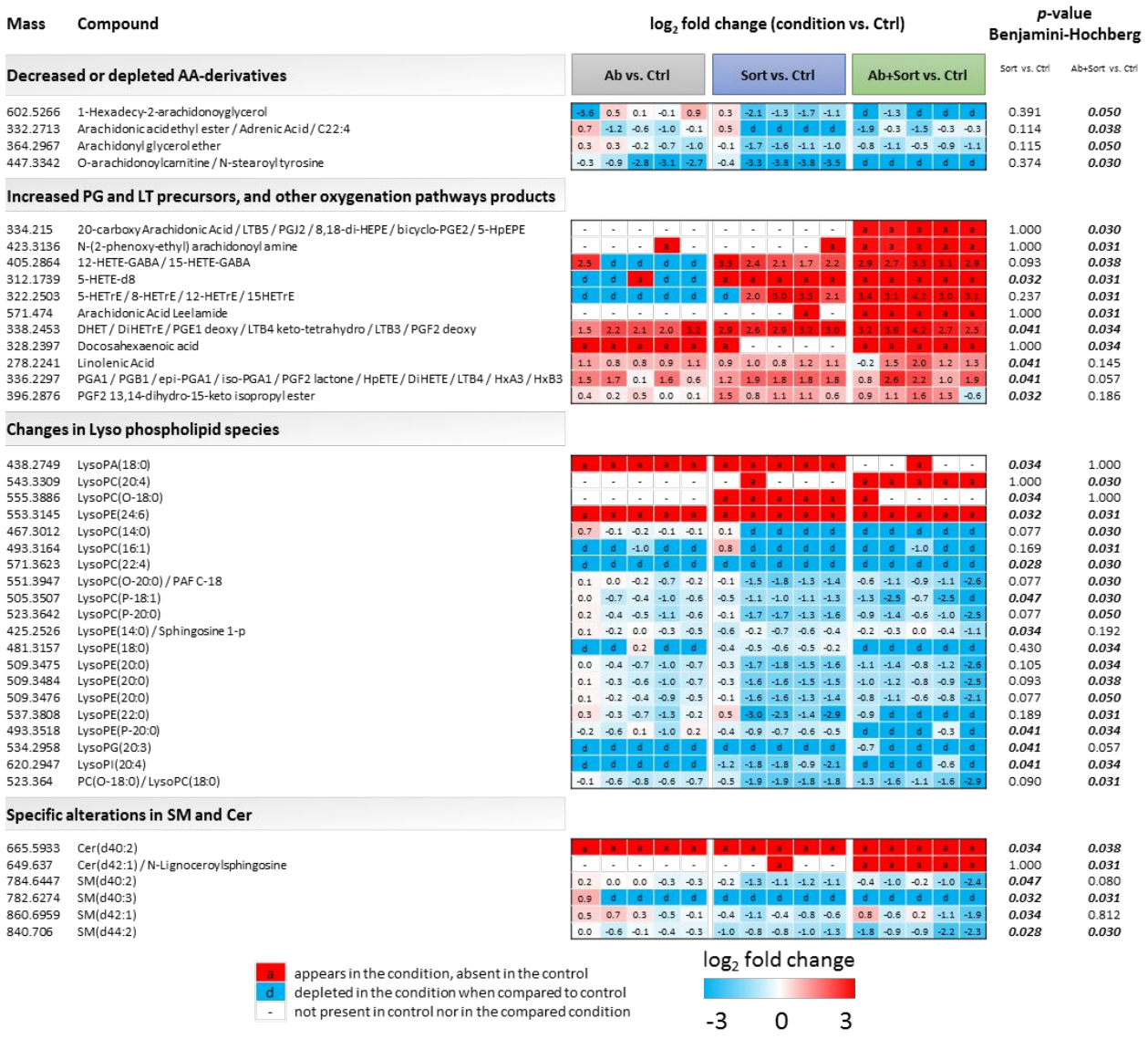
Mass
Compound
log2 fold change (condition vs. Ctrl)
p-value Benjamini-Hochberg
Ab vs. Ctrl
Sort vs. Ctrl
Ab+Sort vs. Ctrl
Sort vs. Ctrl
Ab+Sort vs. Ctrl
Decreased or depleted AA-derivatives
602.5266 1-Hexadecy-2-arachidonoylglycerol 0.391 0.050
332.2713 Arachidonic acid ethyl ester / Adrenic Acid / C22:4 0.114 0.038
364.2967 Arachidonyl glycerol ether 0.115 0.050
447.3342 O-arachidonoylcarnitine / N-stearoyl tyrosine 0.374 0.030
Increased PG and LT precursors, and other oxygenation pathways products
334.215 20-carboxy Arachidonic Acid / LTB5 / PGJ2 / 8,18-di-HEPE / bicyclo-PGE2 / 5-HpEPE 1.000 0.030
423.3136 N-(2-phenoxy-ethyl) arachidonoyl amine 1.000 0.031
405.2864 12-HETE-GABA / 15-HETE-GABA 0.093 0.038
312.1739 5-HETE-d8 0.032 0.031
322.2503 5-HETrE / 8-HETrE / 12-HETrE / 15HETrE 0.237 0.031
571.474 Arachidonic Acid Leelamide 1.000 0.031
338.2453 DHET / DiHETrE / PGE1 deoxy / LTB4 keto-tetrahydro / LTB3 / PGF2 deoxy 0.041 0.034
328.2397 Docosahexaenoic acid 1.000 0.034
278.2241 Linolenic Acid 0.041 0.145
336.2297 PGA1 / PGB1 / epi-PGA1 / iso-PGA1 / PGF2 lactone / HpETE / DiHETE / LTB4 / HxA3 / HxB3 0.041 0.057
396.2876 PGF2 13,14-dihydro-15-keto isopropyl ester 0.032 0.186
Changes in Lyso phospholipid species
438.2749 LysoPA(18:0) 0.034 1.000
543.3309 LysoPC(20:4) 1.000 0.030
555.3886 LysoPC(O-18:0) 0.034 1.000
553.3145 LysoPE(24:6) 0.032 0.031
467.3012 LysoPC(14:0) 0.077 0.030
493.3164 LysoPC(16:1) 0.169 0.031
571.3623 LysoPC(22:4) 0.028 0.030
551.3947 LysoPC(O-20:0) / PAF C-18 0.077 0.030
505.3507 LysoPC(P-18:1) 0.047 0.030
523.3642 LysoPC(P-20:0) 0.077 0.050
425.2526 LysoPE(14:0) / Sphingosine 1-p 0.034 0.192
481.3157 LysoPE(18:0) 0.430 0.034
509.3475 LysoPE(20:0) 0.105 0.034
509.3484 LysoPE(20:0) 0.093 0.038
509.3476 LysoPE(20:0) 0.077 0.050
537.3808 LysoPE(22:0) 0.189 0.031
493.3518 LysoPE(P-20:0) 0.041 0.034
534.2958 LysoPG(20:3) 0.041 0.057
620.2947 LysoPI(20:4) 0.041 0.034
523.364 PC(O-18:0) / LysoPC(18:0) 0.090 0.031
Specific alterations in SM and Cer
665.5933 Cer(d40:2) 0.034 0.038
649.637 Cer(d42:1) / N-Lignoceroylsphingosine 1.000 0.031
784.6447 SM(d40:2) 0.047 0.080
782.6274 SM(d40:3) 0.032 0.031
860.6959 SM(d42:1) 0.034 0.812
840.706 SM(d44:2) 0.028 0.030
a appears in the condition, absent in the control
d depleted in the condition when compared to control
- not present in control nor in the compared condition
log2 fold change
-3 0 3

**Figure 4.**

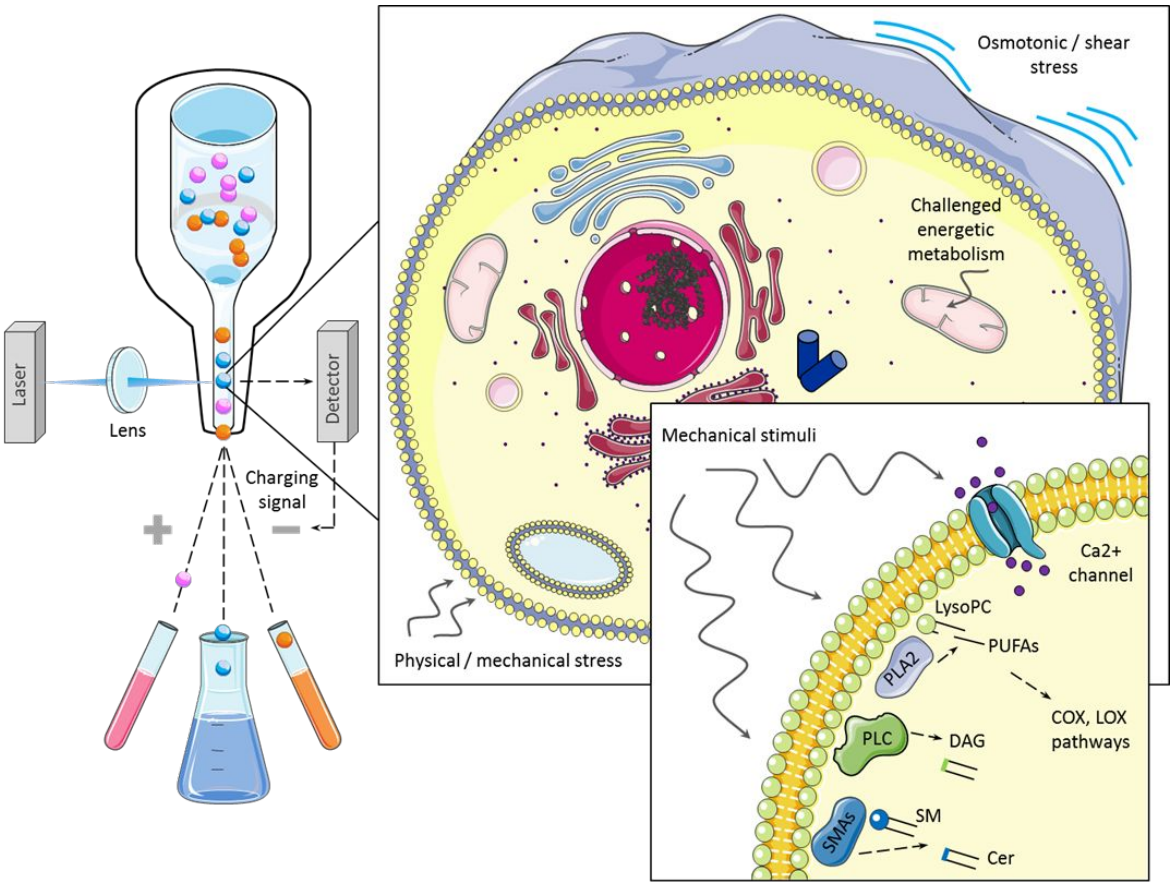
Laser
Lens
Detector
Charging signal
Osmotonic / shear stress
Challenged energetic metabolism
Physical / mechanical stress
Mechanical stimuli
Ca2+ channel
LysoPC
PUFAs
PLA2
COX, LOX pathways
PLC
DAG
SMAS
SM
Cer

**Figure 5.**

**For TOC only**

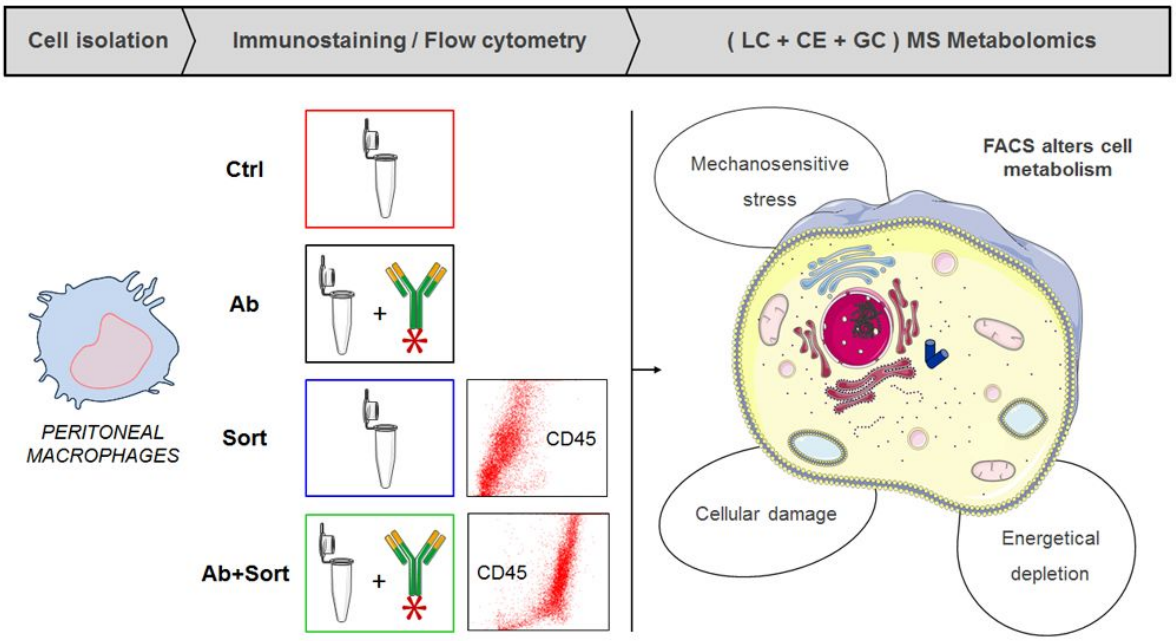
Cell isolation
Immunostaining / Flow cytometry
( LC + CE + GC ) MS Metabolomics
Ctrl
Ab
Sort
Ab+Sort
CD45
CD45
PERITONEAL MACROPHAGES
Mechanosensitive stress
FACS alters cell metabolism
Cellular damage
Energetical depletion

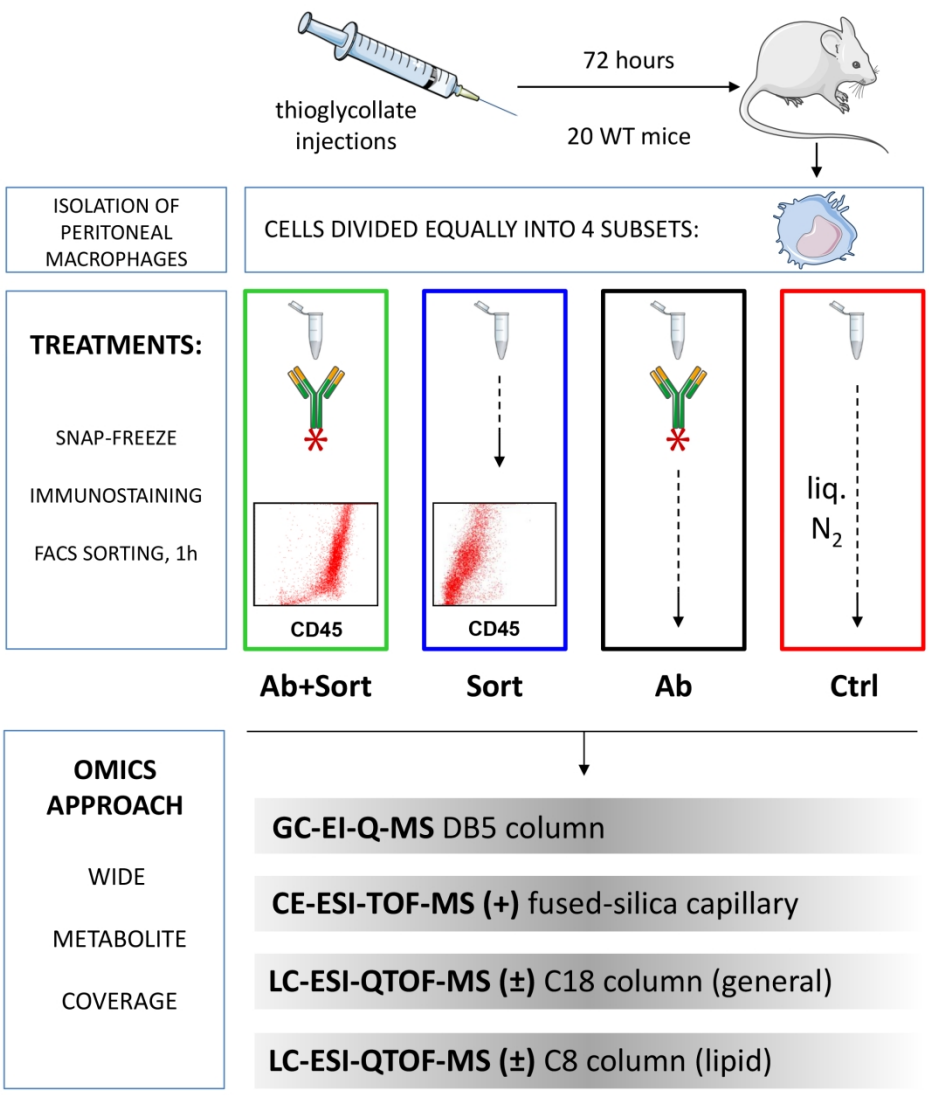


Figure 1. Simplified workflow for the metabolomic study of FACS-sorted peritoneal macrophages. C57BL/6 mice received thioglycollate injections in the peritoneal cavity, and macrophages were collected after 72 h. Cells were counted under a microscope and divided in to 4 equal samples. The cell pellet of the Ctrl experimental group was snap-frozen immediately after isolation. Cells in the Ab samples were resuspended in blocking buffer and incubated with anti-CD16/CD32 and PerCP-Cy5.5-labeled anti-CD45, followed by washing and snap-freezing in liquid N2. The Sort and Ab+Sort samples were prepared according to the protocols for the Ctrl and Ab groups, respectively, but before the final snap-freezing step the cells these 2 experimental groups were subjected to flow cytometry. Metabolites were extracted from all cell pellets with i) MTBE:MetOH and ii) MetOH:H2O, and the resulting supernatants were analysed by GC-EI-QMS, CE-ESI-TOF-MS, and LC-ESI-QTOF-MS in positive and negative ionization modes in 2 chromatographic gradients (general and lipid). Five biological replicates were injected. Quality control (QC) samples were prepared by pooling equal volumes of all metabolite extracts and injected in between blocks of 4 samples until the end of the run to ensure analytical reproducibility.

190x212mm (300 x 300 DPI)

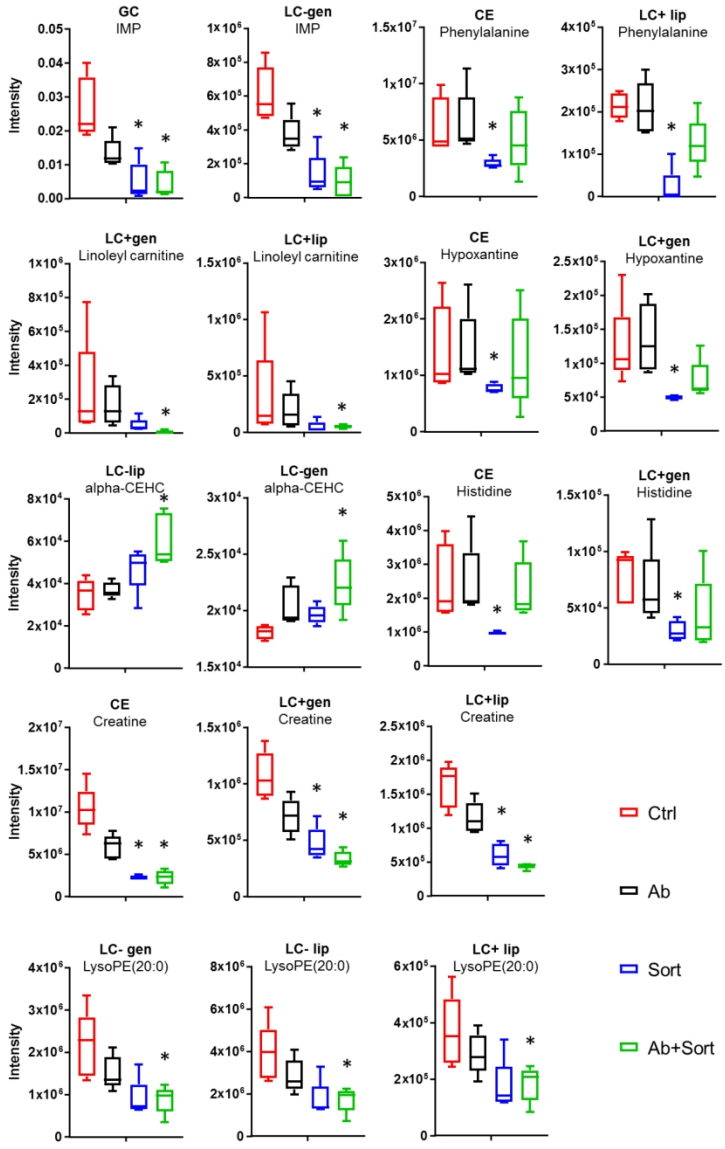


Figure 2. Selected boxplots representing the intensity of annotated metabolites (inosine monophosphate, phenylalanine, linoleyl carnitine, hypoxanthine, alpha-CEHC, histidine, creatine, and LysoPE(20:0)) codetected by different separation techniques. These metabolites were selected to illustrate distinct analytical situations and biochemical classes. The selection covers downregulated metabolites involved in pathways of energy generation, storage, and transfer (creatine, linoleyl carnitine), structural compounds (lysophospholipids), nucleic acid metabolism (hypoxanthine, IMP), and others (alpha-CEHC, histidine). Results are shown as box and whisker plots of minimum to maximum values obtained in 5 replicates. * Indicates p value < 0.05 versus baseline by Mann-Whitney U test followed by Benjamini-Hochberg post hoc correction.

190x254mm (300 x 300 DPI)

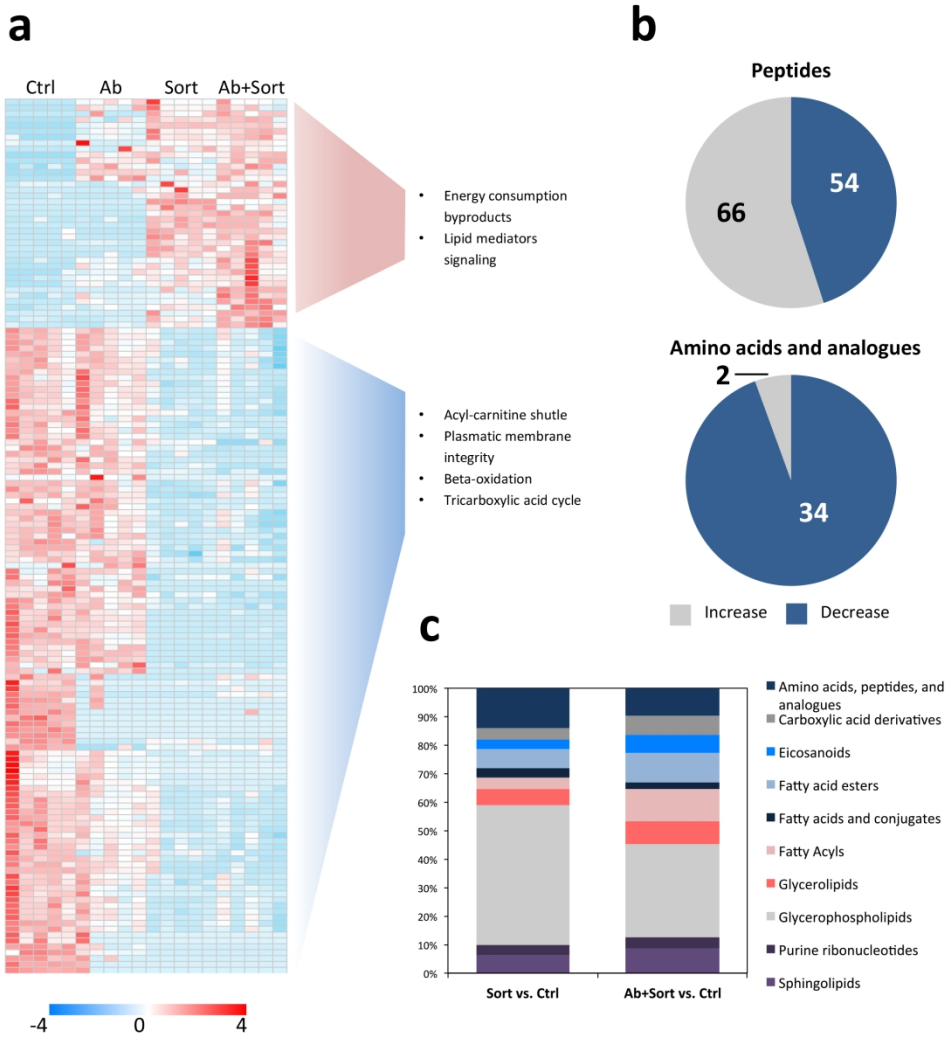


Figure 3. Biochemical classes altered in 3 experimental conditions with respect to the control group (Ctrl): Ab, Sort, and Ab+Sort. (a) Hierarchical clustering analysis of metabolites showing statistically significant alteration. (b) Direction of changes in the subpopulations of amino acids, peptides, and analogues. (c) Biochemical categories (sub-class in HMDB) of metabolites showing statistically significant alteration (Mann-Whitney U test followed by Benjamini-Hochberg post hoc correction, p value < 0.05, n=5) with manually curated identification. For details see Supplementary Figure S5 and Supplementary Table S3.

190x205mm (300 x 300 DPI)

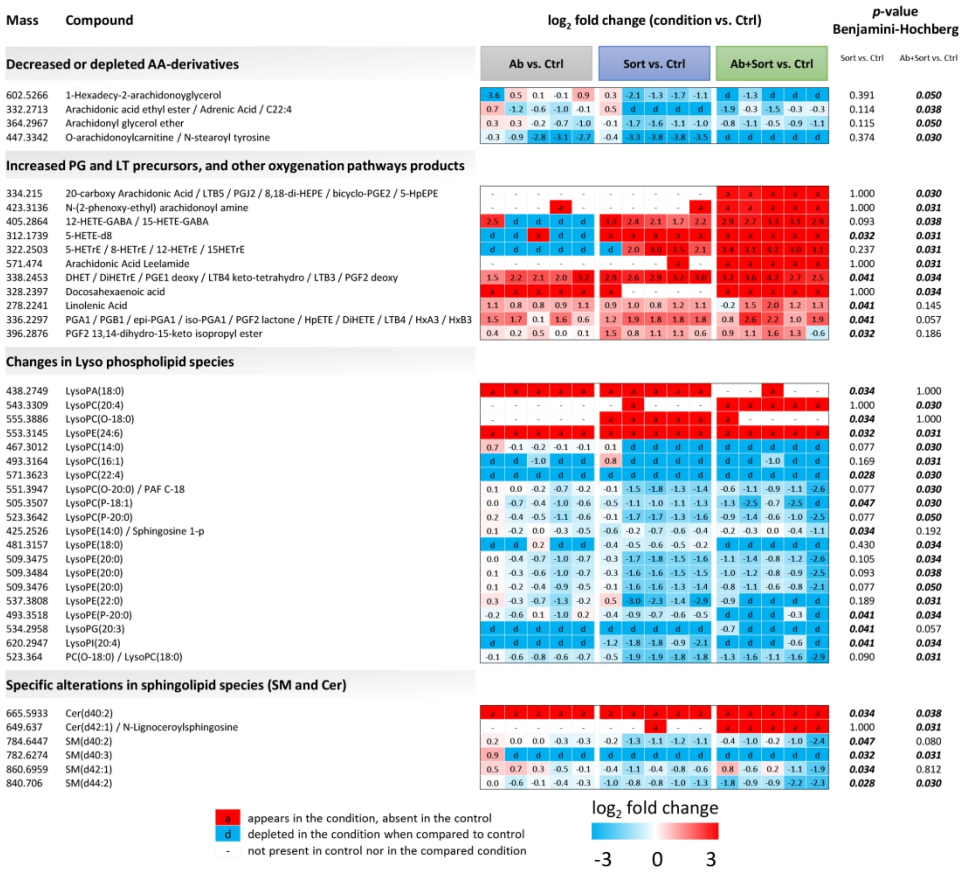


Figure 4. The heatmap represents the log2 fold changes of individual samples intensities in each condition with respect to Ctrl sample average intensity. Selected groups of metabolites with manually curated identification show statistically significant alterations (Benjamini-Hochberg post hoc correction, p value < 0.05 in bold italics). For further details such as individual intensities or separation techniques see Supplementary Table S3

190x176mm (300 x 300 DPI)

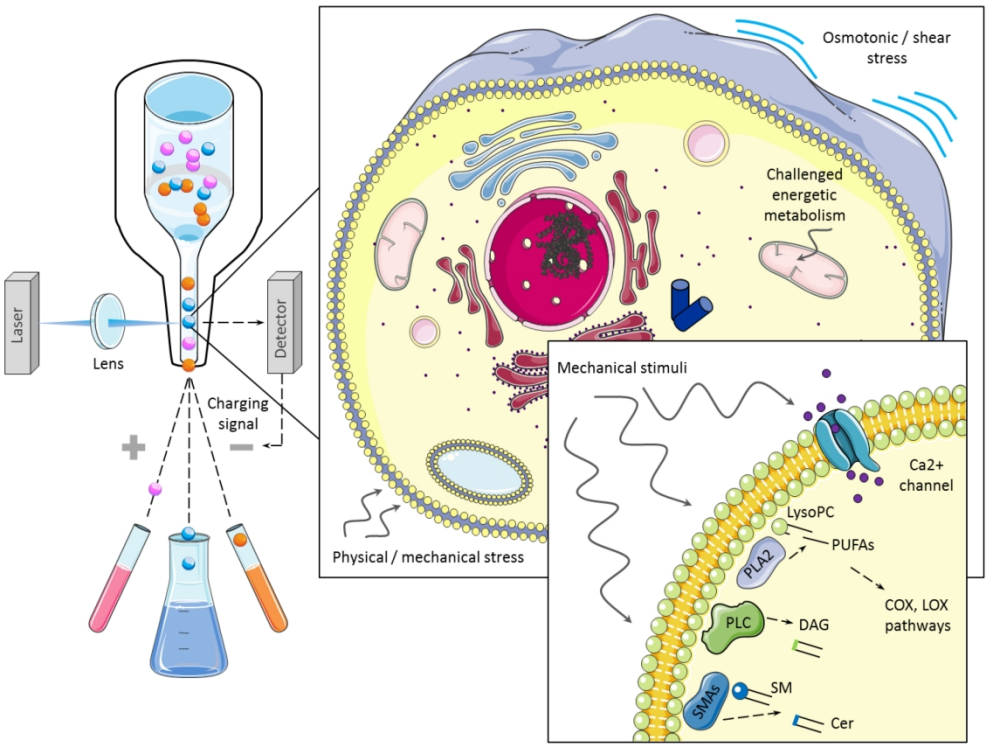


Figure 5. FACS affects cell metabolism. The figure represents some of the main stress inputs, including a graphical summary of the mechanosensitive cascade triggered by mechanical stimulus of the plasma membrane (inset).

190x155mm (300 x 300 DPI)

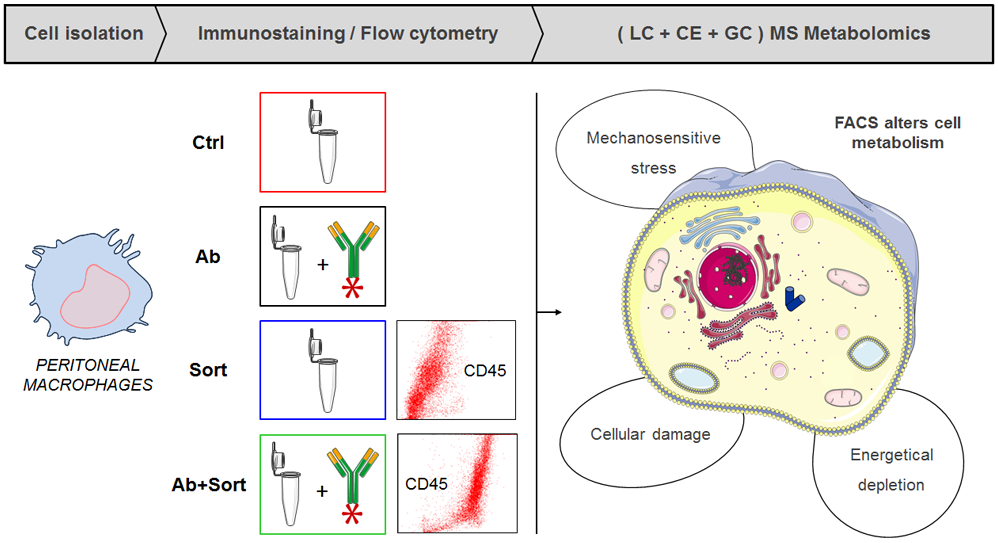


for TOC only

84x47mm (300 x 300 DPI)